P-13-38

System design of Dome plug

Mechanical properties of rock-concrete interface

Mathias Flansbjer, SP Technical Research Institute of Sweden

Jonas Magnusson, NCC Engineering

April 2014

Svensk Kärnbränslehantering AB
Swedish Nuclear Fuel
and Waste Management Co

Box 250, SE-101 24 Stockholm
Phone +46 8 459 84 00

ISSN 1651-4416
SKB P-13-38
ID 1402879

System design of Dome plug

Mechanical properties of rock-concrete interface

Mathias Flansbjer, SP Technical Research Institute of Sweden

Jonas Magnusson, NCC Engineering

April 2014

Keywords: Low pH concrete, Rock-concrete interface, Bond strength, Shear strength.

Abstract

SKB plug reference design concept for closure of the deposition tunnels, where canisters for spent nuclear fuel are deposited, is based on a bentonite sealing layer supported by a spherical concrete dome structure arching between recesses constructed in the rock walls.

In this report the mechanical properties of the interface between the concrete dome and the wire sawn rock surface were investigated. These properties can be used to improve modelling of the rock-concrete interface to determine for instance if the concrete plug will release from the rock during the hardening process of the concrete or through early cooling of the plug.

The mechanical testing was performed on specimens core-drilled from small scale rock-concrete blocks manufactured in the laboratory.

The tensile bond strength of the rock-concrete interface was determined by pull-off tests on cores drilled through the interface and the tensile softening behaviour was evaluated from direct tensile tests on cylinders. The shear strength of the interface and the residual shear strength of the broken interface were determined by shear load tests on cylinders at different constant normal stress levels.

In addition, mechanical properties of the concrete material were evaluated, namely; compressive strength, splitting tensile strength, direct tensile strength and fracture energy.

Sammanfattning

SKBs designkoncept för förslutning av deponeringstunnlar, där kapslarna för använt kärnbränsle deponeras, bygger på ett tätskikt av bentonit och ett mothåll i form av en sfärisk betongplugg som genom valvverkan vilar mot urtag i bergväggen.

I denna rapport har de mekaniska egenskaperna hos gränsskiktet mellan betongpluggen och den wire-sågade bergytan undersökts. Dessa egenskaper kan användas för att förbättra modellering av vidhäftningen mellan berget och betongen för att bland annat bestämma om pluggen kommer att lossna från berget under härdningsprocessen eller genom tidigt kylning av pluggen.

De mekaniska proverna utfördes på cylindrar kärnborrade från småskaliga block bestående av bergblock som motgjutits med betong i laboratoriet.

Vidhäftningshållfastheten för gränsskiktet mellan berget och betongen bestämdes genom dragförsök på kärnor borrade genom gränsskiktet och efterbrottsbeteendet utvärderades från direkta dragprov på cylindrar. Skjuvhållfastheten för gränsskiktet och den kvarvarande skjuvhållfastheten för det brutna gränsskiktet bestämdes genom skjuvförsök på cylindrar vid olika konstanta normalspänningsnivåer.

Vidare bestämdes ett antal mekaniska egenskaperna för betongmaterialet; tryckhållfasthet, spräckhållfasthet, direkt draghållfasthet och brottenergi.

Contents

1 Introduction

1.1 General

SKB plug reference design concept for closure of the deposition tunnels, where canisters for spent nuclear fuel are deposited, is based on a bentonite sealing layer supported by a spherical concrete dome structure arching between recesses constructed in the rock walls.

The structure will endure a high pressure from swelling forces in the backfill clay, at present by introduction of a specially designed backfill transition zone assumed to be confined to approximately 2 MPa. However, due to the uncertainty a backfill swelling design pressure of 4 MPa has been adopted, which also shall be combined with the ground water pressure of about 5 MPa.

The bentonite buffer rings around the deposited canister is sensitive to erosion, which leads to that only a small leakage through the concrete plug is allowed. Even though the final value for the maximum allowed leakage is not yet established, an acceptable leakage value of 0.0025 l/min has been discussed. Awaiting the final design value to be determined the measuring range for the measuring equipment developed for the plug structure has tentatively been selected at 0.0025–0.05 l/min (i.e. approximately 4–70 l/day).

1.2 Objectives

The aim of the investigation was to determine the mechanical properties of the interface between the concrete plug and the wire sawn rock surface. It will contribute to improve the understanding of the interaction between the concrete surface of the plug and the surrounding rock surface. Modelling of the rock-concrete interface can for instance be used to determine if the plug will release from the rock during the hardening of the concrete or through cooling of the concrete plug.

The mechanical testing was performed on specimens core-drilled from small scale rock-concrete blocks manufactured in the laboratory.

The tensile bond strength has been determined by pull-off tests on cores drilled through the rock-concrete interface. The tensile softening behaviour of the interface was evaluated from direct tensile tests on cylinders. The shear strength of the interface and the residual shear strength of the broken interface were determined by shear load tests on cylinders at different constant normal stress levels.

In addition, mechanical properties of the concrete material were evaluated, namely; compressive strength, splitting tensile strength, direct tensile strength and fracture energy. These properties can be used to model and better understand the structural behavior of the concrete plug under loading.

2 Test preparation

The mechanical testing of the rock-concrete interface was performed on specimens that were core-drilled from rock-concrete blocks. The blocks were manufactured in the laboratory of SP Building Technology and Mechanics, by casting concrete against the wire sawn surfaces of rock panels.

2.1 Rock panels

Five rock panels with wire sawn surfaces were delivered to SP from the Äspö laboratory, see Figure 2-1. The panels had been sawn out of two rock blocks and the sawn surfaces were denoted 1a, 1b, 1c and 1d for block #1 and 2a and 2b for block #2. One panel had two sawn surfaces. Fibreboards were placed between the panels to protect the sawn surfaces during the transportation. The dimensions of the panels were approximately 800×700×150 mm.

The characteristics of the wire sawn surfaces were documented with optical 3D-scanning, see Figure 2-2. The scanning was performed by Cascade with the measuring system ATOS Triple Scan from GOM. To get a high local resolution, the surfaces were divided into subareas of approximately 350×350 mm, giving a point spacing of approximately 0.1 mm. The ATOS measurements of the individual subareas were then combined with TRITOP 3D coordinate measurements to give a complete description of the entire surface. Characteristics of the wire sawn rock surfaces can be found in Appendix A.

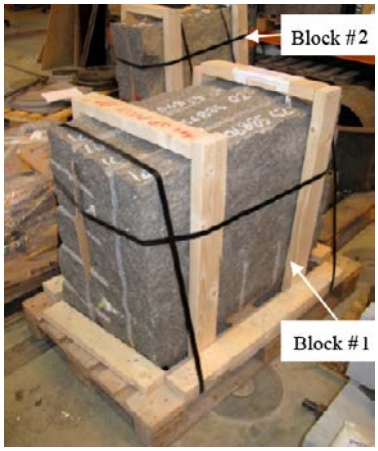

Figure 2-1. *Photo of rock panels delivered from Äspö laboratory.*

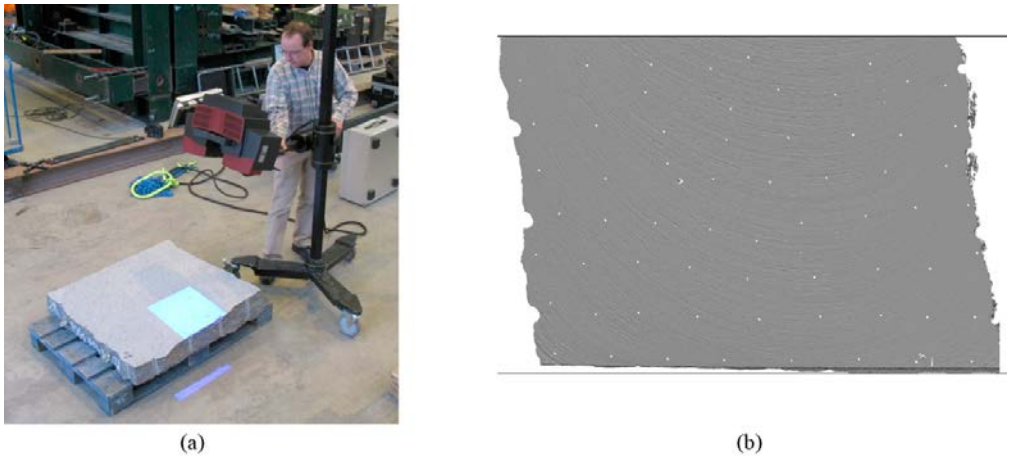

Figure 2-2. *a) Photo of 3D-scanning of a wire sawn rock panel surface and b) illustration of scanning results.*

2.2 Concrete mix

The concrete was manufactured at the laboratory of CBI Swedish Cement and Concrete Research Institute. The concrete mix composition and mixing order of the low pH SCC B200 were in accordance to the specifications reported in Vogt et al. (2009), see Table 2-1 and Table 2-2, respectively. The coarse aggregate (8–16 mm) used in this project was crushed granite from the Gothenburg area. The fine aggregate (0–8 mm) was natural sand taken from same source in the Äspö area as used in Vogt et al. (2009). The concrete was mixed in a forced action mixer for a total time of approximately 10 minutes. The concrete had a slump flow value of approximately 700 mm. Concrete cubes (150×150×150 mm) and cylinders (Ø150×300 mm) were cast for determination of the compressive strength.

Table 2-1. Composition of concrete mix B200.

Constituents	Manufacturer	Quantity [kg/m^3]	
		Design mix	Final mix
CEM I 42.5	Cementa	120	120
Silica fume	Elkem	80	80
Water		165	164
Limestone filler Limus 25	Nordkalk	369	368
Sand 0–8 mm	Fogelheim 6:2	1037	1028
Gravel 8–16 mm		558	548
Glenium 51	BASF	6.38	6.00
Water/cement		1.375	1.367
Water/binder		0.825	0.820
Water/powder		0.290	0.289

Table 2-2. Mixing order of B200 in the laboratory test.

Sequence	Activity
1	Aggregates and silica fume
2	Mixing
3	Cement and limestone filler
4	Mixing
5	Water and superplasticizer
6	Final mixing

2.3 Manufacturing of rock-concrete blocks

The rock-concrete blocks were manufactured in moulds made of shuttering plywood, see Figure 2-3. The moulds were prepared with plastic foil (Mataki Teno air and vapour barrier) to prevent moisture departure from the concrete. The wire sawn surface at the rock panel was orientated to be parallel to the final concrete surface from where the drilling was going to be performed, i.e. the drilling axis becomes perpendicular to the rock-concrete interface. Any loose particles were removed from the rock surface. The rock surfaces were kept wet for approximately 24 hours, after which all excess water was removed before casting. Schematic illustrations of the manufactured rock-concrete blocks are shown in Figure 2-4. In total, five rock-concrete blocks were manufactured. In four blocks, the concrete was cast on top of a horizontal rock surface (1a, 1d, 2a and 2b). The two sided sawn rock panel was placed in an upright position and the concrete was cast against the vertical rock surfaces (1b and 1c) on either side of the panel. In addition, two blocks of plain concrete were cast for preparation of material test specimens. After casting, the free concrete surfaces were covered with a moist micro-fiber fabric and a plastic foil. The day after casting the samples were enclosed by the plastic foil and sealed with splicing tape (Mataki Teno Tape). After preparation the blocks were stored at a temperature of approximately 20°C.

(a) (b)

Figure 2-3. *Photo of rock panels placed in the in the moulds before casting. The casting was performed a) against a horizontal surface and b) against vertical surfaces.*

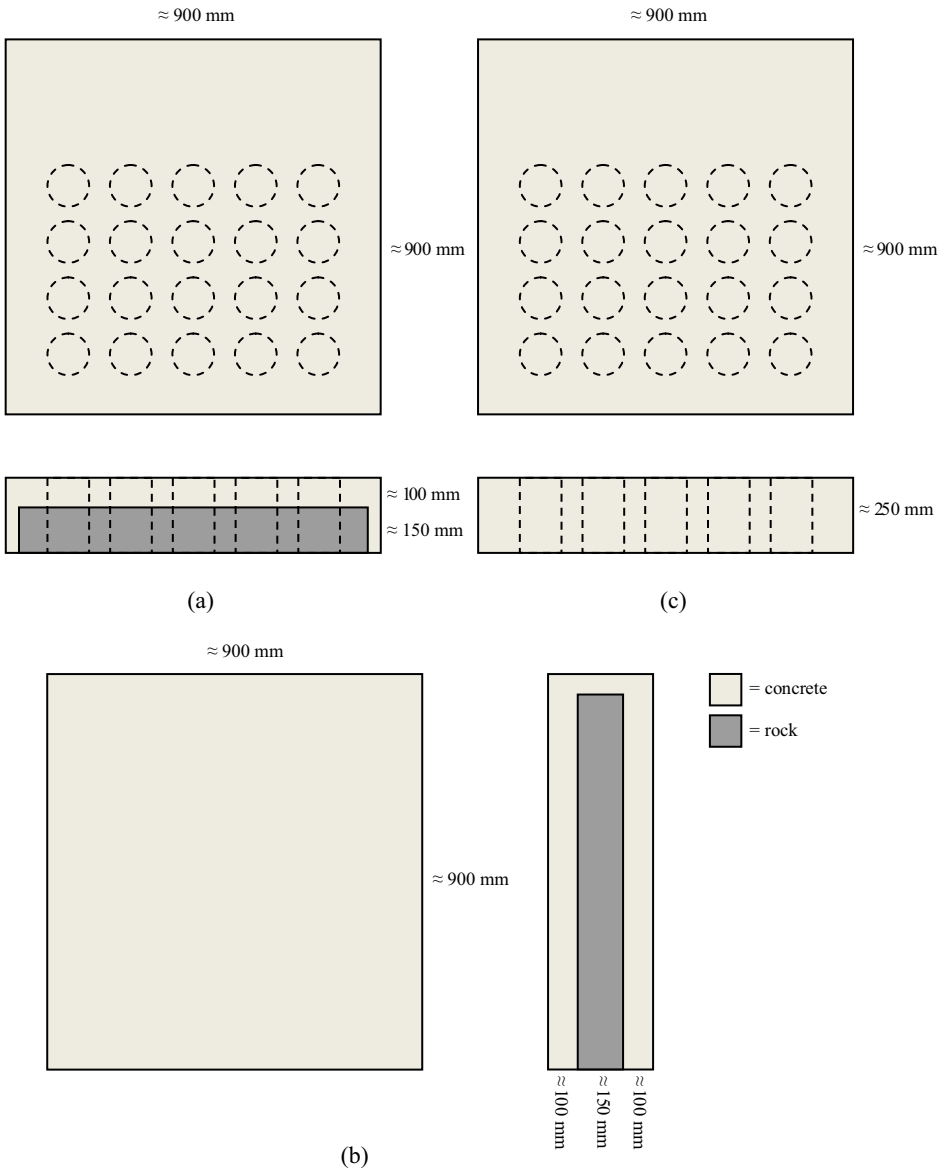

Figure 2-4. *Schematic illustration of a) horizontal rock-concrete block, b) vertical rock-concrete block and c) plain concrete blocks.*

3 Description of test methods

3.1 Tensile bond strength

The tensile bond strength between the rock and the concrete has been determined by pull-off tests using a loading plate bonded to the surface of cylinders cored through the rock-concrete interface.

The test positions were evenly distributed over the test sample. The surface at each test position was grinded to achieve good bonding to the adhesive. The drilling equipment was fixed to the top of the concrete layer in order to get a drill axis perpendicular to the surface and to minimize the vibration and the lateral movement of the coring bit. A diamond core drill was used to drill Ø50 mm cylinders through the concrete and approximately 3–4 mm into the rock. The cores were drilled on the day before testing to ensure a dry surface for gluing. A circular loading plate made of steel with a diameter of Ø50 mm was glued concentrically to the top of each cylinder. The adhesive used was X60 by HBM. The adhesive was allowed to set for at least one hour before testing.

The tensile bond strength test was carried out using an EASY M type F10D pull-off test equipment made by FREUNDLER, with a load rate of 0.05 MPa/s, see Figure 3-1. The pull-off equipment was placed concentrically over the loading plate and with a loading axis perpendicular to the cored surface. The attaching mechanism to the loading plate includes a spherical seat, to ensure that the load is applied normal to the surface under the test, without bending or shear forces being applied to the test area. The spherical seat is placed approximately 40 mm from the surface of the loading plate. The equipment is provided with a measurement device that retains the reading of the maximum force exerted. The tensile bond strength was calculated as the failure load divided by the area of the cylinder at the failure face.

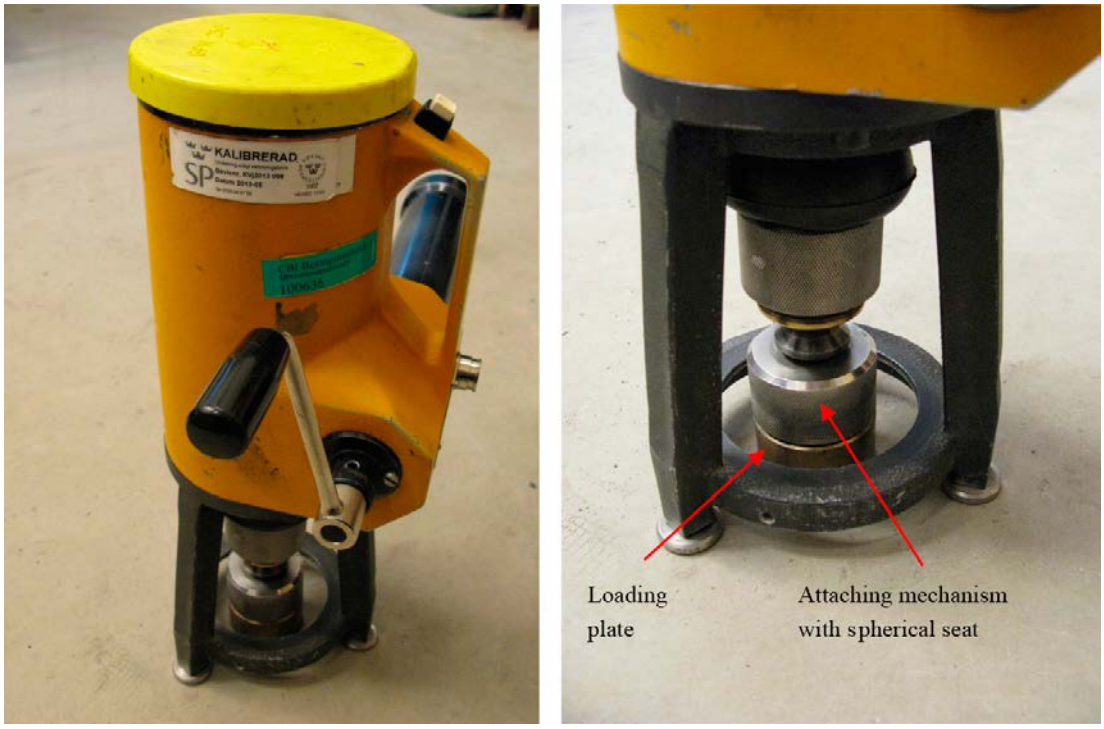

Figure 3-1. *Photos of pull-off test equipment.*

3.2 Direct tensile tests

The softening behaviour of the concrete material and the rock-concrete interface were obtained from direct tensile tests, performed on cylinders with fixed end conditions following the recommendations given in RILEM (2001, 2007). For the rock-concrete joint specimens the crack propagation at the interface was also registered in a detailed way by the use of optical full-field deformation measurements.

3.2.1 Preparation of tensile test specimens

Cylinders with a diameter of 100 mm were core-drilled from the concrete blocks and the rock-concrete blocks described in Section 2. The cores were cut to a length slightly more than 100 mm, after which the top and bottom edges were face-ground down to approximately 100 mm. The rock-concrete joint was approximately located in the centre of the final specimen.

Around the mid-section of the concrete cylinders a 10 mm deep and 5 mm wide notch was cut.

The notch was cut with a stationary diamond cutting-blade with the cylinder fixed in one position, but rotated around its centre axis until the desired notch depth was achieved. The diameter across the notch and the joint was measured at three separate locations along the perimeter; the average was used to calculate the cross sectional area at the notch and joint, respectively. The geometries of the specimens are shown in Figure 3-2.

The specimen was glued to the lower loading platen using a "glue device" which ensured the centre lines of the platen and the cylinder to coincide and in order to ensure perpendicularity between the face of the loading platen and the centre axis of the specimen as close as possible, see Figure 3-3. The lower loading platen, together with the glued on specimen, is then bolted to the machine. Finally, the upper loading plate, which was already attached to the machine, was glued to the top of the specimen. Any small deviation from parallelism between the end surface of the specimen and the loading platen are accommodated by the adhesive layer yielding a perfect fit between the specimen and the loading platens. The maximum difference in adhesive thickness over the area was approximately 0.1 mm i.e. deviation from the cylinder edges being parallel. The adhesive used was X60 by HBM. The adhesive was allowed to set for at least 30 minutes before testing.

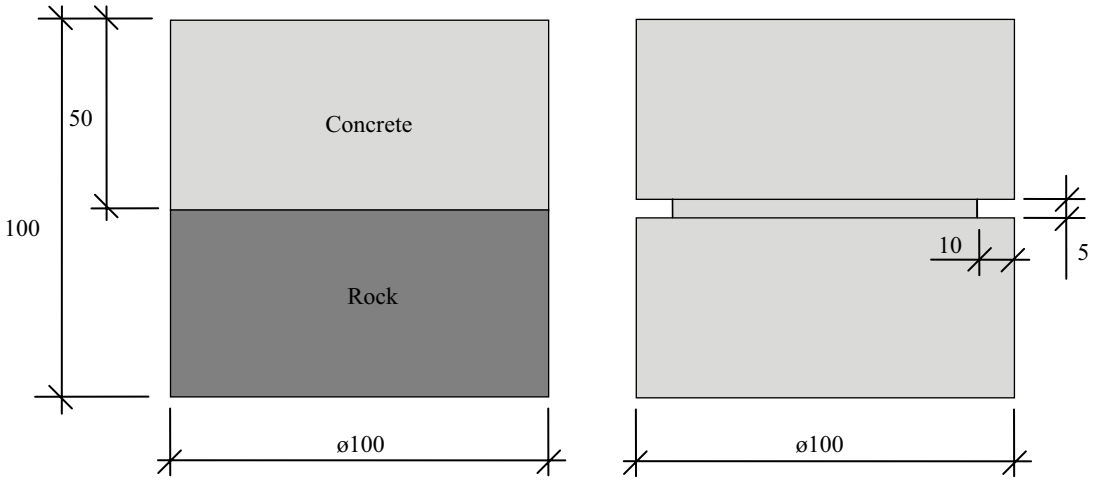

Figure 3-2. *Tensile test specimen geometry.*

Figure 3-3. *Photo of the "glue device" (with lower loading platen in upper part of picture).*

3.2.2 Direct tensile test setup and performance

The direct tensile test setup was based on the test method recommended for concrete described in RILEM (2001, 2007), see Figure 3-4. The tests were conducted using a moment stiff loading device in order to suppress rotations of the holders that could lead to bending failure. The device was pre-tensioned with a load of 150 kN. The tests were displacement controlled and carried out in a GCTS servo-hydraulic machine with a stiff load frame. The load cell used was rated up to 200 kN. The accuracy of the load measurement is within 1%. The displacement was measured locally over the notch or joint with three inductive displacement transducers with a gauge length, l_g, of 31 mm. The transducers had a measuring range of ±2.50 mm and a relative error less than 1%. The gauges were approximately centered over the location of the notch or joint. The mean value of the three displacement values was used for the displacement control. The displacement was applied at a rate of 0.005 mm/min up to a displacement of $\delta = 0.1$ mm and then increased to 0.1 mm/min for the remaining part of the test.

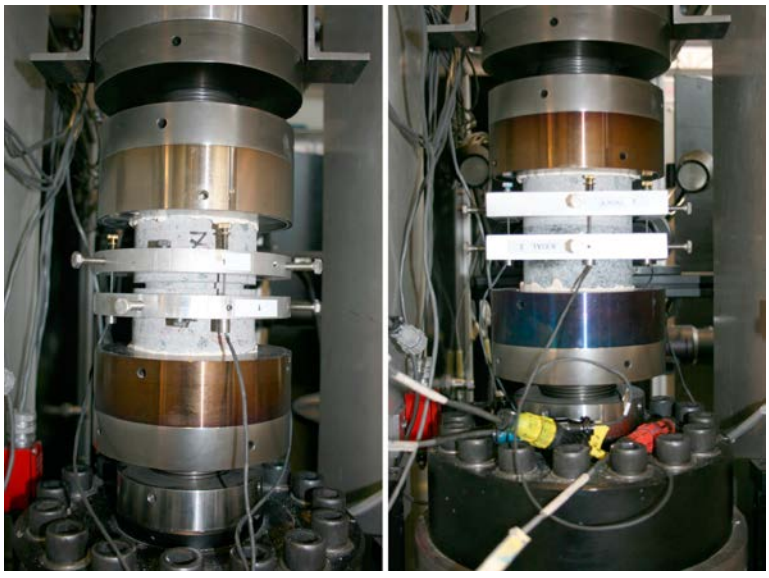

Figure 3-4. *Experimental test setup for the direct tensile tests on a) the concrete material and b) the rock-concrete interface.*

The crack opening w, in the post-peak regime, was evaluated according to RILEM (2007) by subtracting the elastic deformation δe from the measured displacement δ as:

$$w = \delta - \delta_e = \delta - \frac{\sigma}{E} l_g = \delta - \frac{\sigma}{K} \quad (3\text{-}1)$$

where σ is the tensile stress, E is the modulus of elasticity and l_g is the gauge length. Since the notches and the interface hamper the direct measurement of the modulus of elasticity in tension, the ratio E/l_g was replaced by the elastic stiffness K, which was evaluated directly from the tensile stress-displacement relations. The fracture energy, G_F, was calculated from the area under the stress-crack opening curve as:

$$G_F = \int \sigma(w)\, dw \quad (3\text{-}2)$$

3.2.3 Full field deformation measurements

For the rock-concrete joint specimens the crack propagation was registered during the testing by the use of the optical full-field deformation measurement system ARAMIS™ 4M by GOM. The system uses a measurement technique based on Digital Image Correlation (DIC) with a stereoscopic camera setup, consisting of two CCD-cameras with 4.0 Mega pixel resolutions. The basic idea behind DIC is to measure the displacement of the specimen under testing by tracking the deformation of a natural occurring, or applied surface speckle pattern in a series of digital images acquired during the loading. This is done by analyzing the displacement of the pattern within discretized pixel subsets or facet elements of the image. In combination with correlation based stereovision technique the measurement of 3D shapes as well as the measurement of 3D displacements fields and surface strain field is possible.

The experimental setup of the system can be seen in Figure 3-5. The cameras, which are mounted on a rigid bar to avoid motion relative to each other, are placed in front of the specimen at angles and a distance, both of which depend on the desired measuring volume and the lenses used. In this study the system was calibrated for a measurement volume of approximately 100×100×80 mm. To obtain high contrast levels the specimen was illuminated by a white light. In the tests an image pair was captured with two seconds intervals; at the same time the load and displacement, obtained from the testing machine, were recorded in the ARAMIS system.

In this study a facet size of 15×15 pixels and a two-pixel overlap along the circumference of each facet were chosen. For the system setup employed this corresponds to a spatial resolution of approximately 0.7×0.7 mm. The coordinate measurement accuracy was approximately 2 µm.

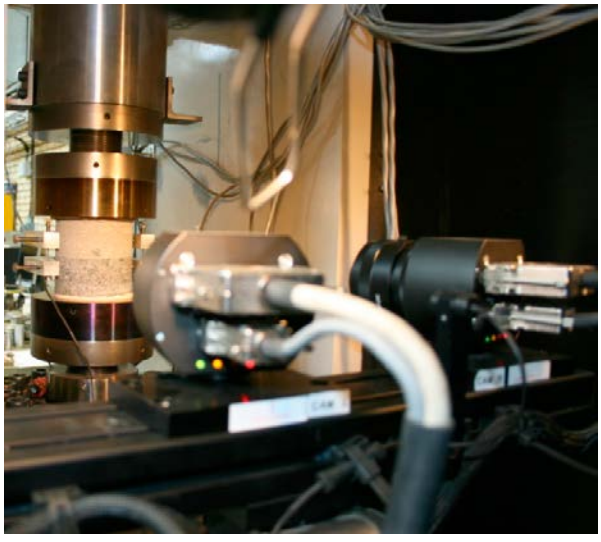

Figure 3-5. *Experimental test setup, where optical strain measurement system is seen in the foreground.*

3.3 Direct shear tests

The behaviour of the interface between the rock and the concrete was investigated by shear loading tests on six specimens, tested at different constant normal stress levels. The aim was to determine the peak shear stress when the rock-concrete joints fail and the following residual shear stress. For two of the samples the broken joints were also subjected to shear loading cycles at various normal stress levels.

3.3.1 Preparation of shear test specimens

Cylinders with a diameter of approximately 80 and 65 mm were core-drilled from the rock-concrete blocks described in Section 2. The cores were cut to a final length of 100 mm, with the joint plane approximately located in the centre of the final specimen, see Figure 3-6. The diameter across the joint was measured at three separate locations along the perimeter; the average was used to calculate the cross sectional area at the joint.

Each specimen was fixated into one lower and one upper steel holder using fast setting cement, such that the joint plane was centred in the opening between the holders, see Figure 3-7. The first half of the specimen was cast in by pouring the cement into the lower holder with the specimen held in correct positioned by a fixture. After one hour of curing, the upper holder was mounted on top of the lower holder with a spacer, creating a gap of 10 mm between the two holders. The second half of the specimen was cast in by pouring cement into the upper holder. The cement was fully hardened after one day in room temperature.

Figure 3-6. *Photo of shear test specimens.*

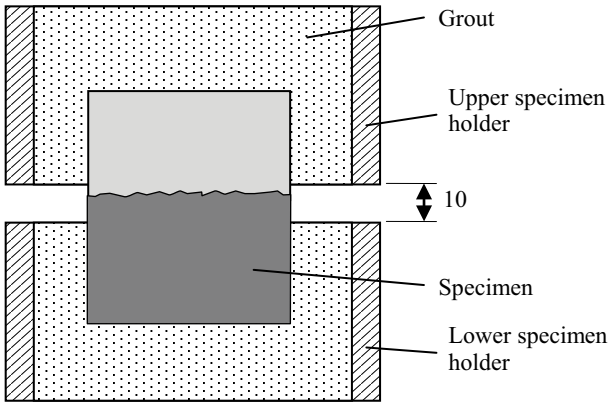

Figure 3-7. *Illustration of specimen cast in the specimen holders.*

3.3.2 Direct shear test setup and performance

The tests were carried out in a GCTS servo-hydraulic machine designed for direct shear testing, see Figure 3-8. The machine is supplied with two shear boxes, one upper and one lower.

The upper box can be moved vertically and the lower box horizontally. Two actuators, one acting vertically and one acting horizontally, are used to apply the forces in the two directions. The horizontal cylinder is connected to a slide which is in turn carried on two linear bearings, guaranteeing linear motion with low friction. The maximum stroke is 100 mm in the vertical direction and ±50 mm in the shear direction.

In the shear test the normal and shear displacements are measured by means of LVDTs. The normal displacement between the shear boxes is measured by four LVDTs, positioned in a square pattern around the specimen, one in each corner. Each of the LVDTs has a measurement range of ±2.5 mm and a relative error less than 1%. The average value of these four LVDTs is used to represent the normal displacement. The relative displacement between the shear boxes in the shear direction is measured by one LVDT, which has a 10 mm range and a relative error less than 1%. The maximum normal load that can be applied is 300 kN and the maximum load in the shear direction is ±300 kN. Load cells are used to measure the forces in both directions. The accuracy of the load measurement is within 1%. The machine is connected to a digital controller with a computer interface for setting up and running tests.

The specimen holder was mounted in the shear boxes in the testing machine. A normal load corresponding to a given normal stress was applied according to the test schedule. The loading rate was 5 MPa/min during normal loading and unloading stages. Subsequently, the normal stress was kept constant and the specimen was sheared by applying a constant shear displacement rate of 0.1 mm/min on the shear actuator.

For two specimens, seven successive shear cycles (s1–s7) were conducted on the broken joint with various constant normal stress levels. Each shear cycle was finished by unloading the shear stress to zero. The normal stress was then lowered to 0 MPa before the shear position was restored to its starting point (zero shear displacement) for the following shear cycle.

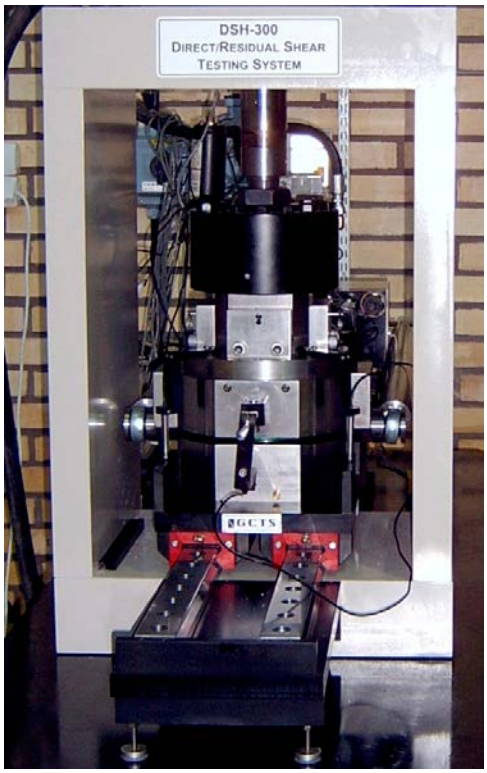

Figure 3-8. *Equipment for direct shear testing.*

4 Test results and evaluation

4.1 Concrete material properties

In this study, following mechanical properties of the concrete material were evaluated; compressive strength (f_{cm}), splitting tensile strength ($f_{ctm,sp}$), direct tensile strength (f_{ctm}) and fracture energy (G_F). A summary of the concrete properties can be found in Table 4-1. Detailed information of the material test results can be found in Appendix B.

The compressive strength was determined using cubes 150×150×150 mm ($f_{cm,cube}$) and cylinders Ø150×300 mm ($f_{cm,cyl}$) according to SS-EN 12390-3:2009. The specimens were stored in water at temperature of approximately 20°C.

The compressive strength and the splitting tensile strength were determined at different ages using cored specimens Ø100×100 mm according to SS-EN 12504-1:2009 and SS-EN 12390-6:2009, respectively. All cored specimens were taken from the plain concrete blocks described in Section 2.3. The specimens were drilled and prepared the day before testing. The develop-ment of the compressive strength and the tensile splitting strength is shown in Figure 4-1.

The material characteristics in tension were evaluated by using two different methods. In the first method, the tensile strength was determined using cored specimens Ø65×100 mm according to CBI-method nr 6, which is based on SS 137231:2005. In this method the loading platens are free to rotate by the use of hinged connections. In the second method, the tensile strength and the softening behaviour of the concrete were evaluated from direct tensile tests, performed on notched core specimens Ø100×100 mm with fixed end conditions as described in Section 3.2.The tensile stress-crack opening relations are shown in Figure 4-2. The fracture energy was calculated from the area under the stress-crack opening curve; see Table 4-1.

Table 4-1. Summary of concrete properties, given as mean values and standard deviations in brackets.

Property	Unit	Specimen	Age [days]		
			12	29	90
$f_{cm,cube}$	[MPa]	cube 150×150×50	–	–	81.9 *(2.2)*
$f_{cm,cyl}$	[MPa]	cylinder Ø150×300	–	–	78.0 *(0.6)*
f_{cm}	[MPa]	core Ø100×100	33.7 *(0.5)*	55.1 *(0.9)*	82.2 *(1.2)*
$f_{ctm,sp}$	[MPa]	core Ø100×100	3.3 *(0.2)*	4.3 *(0.3)*	5.5 *(0.4)*
f_{ctm} [1)]	[MPa]	core Ø65×100	–	–	3.2 *(0.4)*
f_{ctm} [2)]	[MPa]	core Ø100×100	–	–	3.6 *(0.2)*
G_F	[N/m]	core Ø100×100	–	–	121 *(15)*

[1)] Obtained from core specimens Ø65×100 mm with hinged end conditions.

[2)] Obtained from notched core specimens Ø100×100 mm with fixed end conditions.

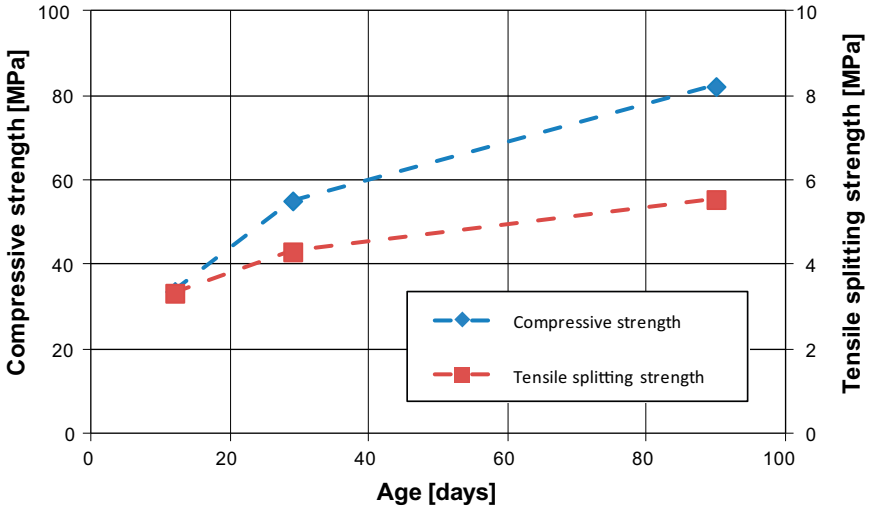

Figure 4-1. *Development of compressive strength and tensile splitting strength, both determined from core specimens Ø100×100 mm.*

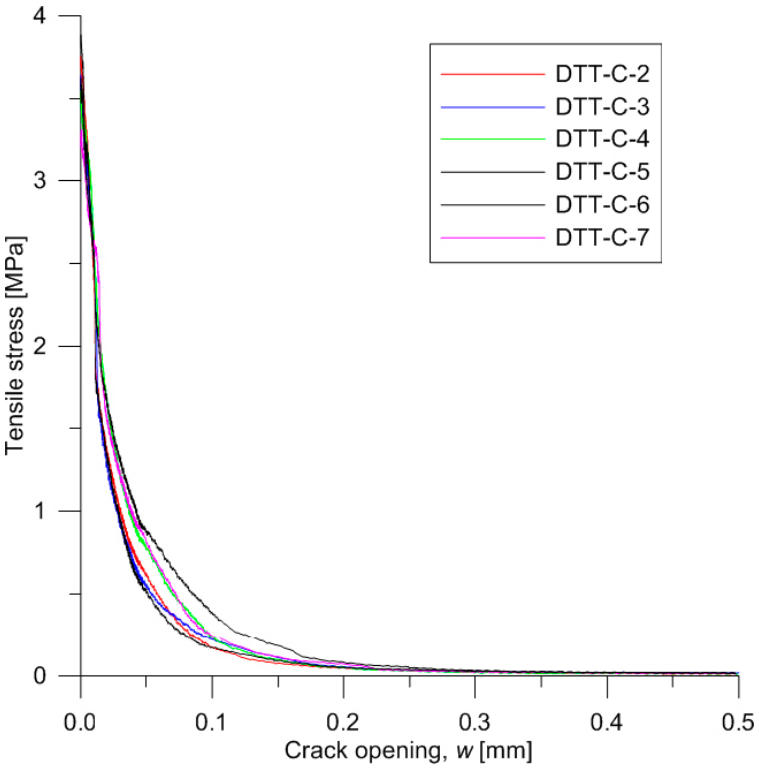

Figure 4-2. *Tensile stress vs. crack opening from direct tensile tests on notched concrete specimens (DTT-C-#).*

4.2 Rock-concrete interface properties

4.2.1 Tensile behaviour

The tensile bond strength at the rock-concrete interface was determined at three different ages by pull-off tests on Ø50 mm cores drilled through the rock-concrete interface as described in Section 3.1. The tests were performed on one interface where the concrete was cast on top of a horizontal rock surface (Horizontal interface 1a) and one where the concrete was cast against a vertical rock surfaces (Vertical interface 1c). A summary of the pull-off test results can be found in Table 4-2 and detailed information in Appendix C.

Table 4-2. Summary of results from the tensile bond strength tests, given as mean values and standard deviations in brackets.

Property	Age [days]	Peak tensile stress [MPa]	Tensile bond strength [MPa]
Vertical interface 1c	12	– [1)]	– [1)]
	30	2.66 (*0.55*)	2.51 (*0.51*)
	91	3.00 (*0.48*)	2.90 (*0.42*)
Horizontal interface 1a	12	1.45 (*0.04*)	1.48 (–) [2)]
	33	3.31 (*0.29*)	3.37 (*0.14*)
	91	4.25 (*0.23*)	4.38 (*0.28*)

[1)] Interface failure at drilling – no results.

[2)] Only one result.

The peak tensile stress includes all tests where the failure occurred at the interface or in the concrete, whereas the tensile bond strength is restricted to the results where the failure occurred at the interface. No results were obtained at the age of 12 days for the vertical interface 1a, since the interface failed already when the cores where drilled through the interface. The development of the peak tensile stress is shown in Figure 4-3. The peak tensile stress was chosen since the statistical basis was bigger; however, there is a good correlation between the peak tensile stress and the bond strength. There is a significant difference in bond strength between the vertical interface and the horizontal interface. For the specimens taken from the vertical interface 1c the majority of the failures occurred at the interface, while for the specimens taken from the horizontal interface 1a the majority of the failures instead occurred in the concrete. The lower bond strength together with the interface failures suggests that the bond is weaker when the concrete is cast against a vertical rock surface.

The tensile bond strength, together with the tensile softening behaviour of the interface, was also evaluated at an age of 90 days, from direct tensile tests on six core specimens Ø100×100 mm with fixed end conditions as described Section 3.2. The specimens were core-drilled from the rock-concrete block 2a, where the concrete was cast on top of a horizontal rock surface. The tests were conducted at an age of 93–97 days. A summary of the direct tensile test results can be found in Table 4-3 and detailed information in Appendix C.

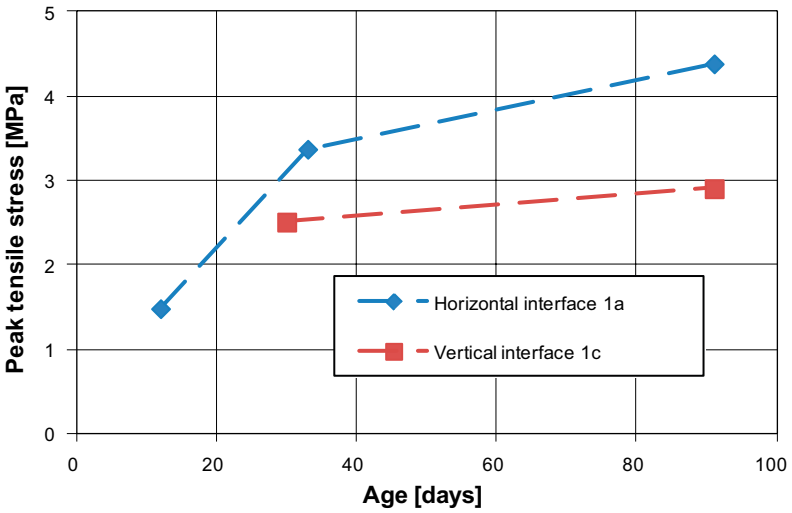

Figure 4-3. *Development of peak tensile stress.*

Table 4-3. Results from direct tensile tests on rock-concrete interface specimens.

Specimen	Area [cm^2]	Age [days]	Failure mode	Peak tensile stress [MPa]	Tensile bond strength [MPa]	Fracture energy [N/m]
DTT-RCI-2	77.8	93	Interface	3.6	3.6	25.8
DTT-RCI-3	77.8	93	Interface	3.8	3.8	–
DTT-RCI-4	77.8	93	Interface	3.7	3.7	26.8
DTT-RCI-5	77.8	97	Concrete	4.1	–	–
DTT-RCI-6	77.9	97	Interface	3.9	3.9	–
DTT-RCI-7	77.8	97	Interface	4.0	4.0	–
			Mean	***3.9***	***3.8***	***26.3***
			Std. dev.	***0.2***	***0.1***	***0.7***

The failure occurred at the interface in all cases except in one, where it occurred in the concrete outside the measuring range, close to the loading plate. In the former cases, the results from the optical full-field deformation measurements confirmed that the cracking was restricted to the interface without major cracking in the concrete, see Appendix C. Comparing the results from the direct tensile tests with fixed end conditions, it can be seen that the tensile bond strength of the horizontal interface (Table 4-3) is at the same level as the tensile strength of the concrete (Table 4-1). The failure of the interface was very brittle and it was only possible to evaluate the stress-crack opening relation and fracture energy for two of the tests, see Figure 4-4 and Table 4-3. It can be noted that the fracture energy from the rock-concrete interface cracking is about 1/5 of the concrete fracture energy stated in Section 4.1.

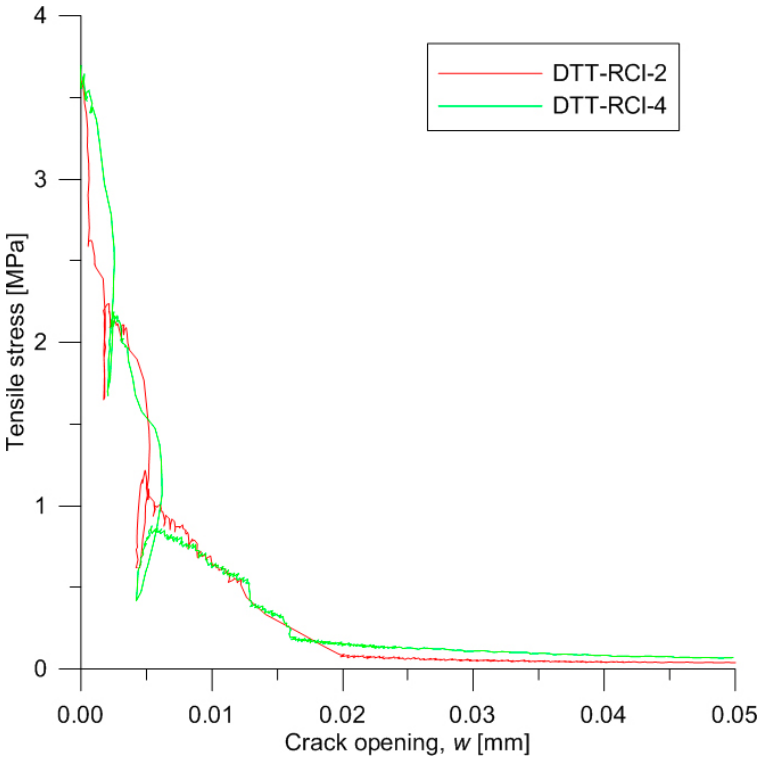

Figure 4-4. *Tensile stress vs. crack opening from direct tensile tests on rock-concrete interface specimens (DTT-RCI-2 and DTT-RCI-4).*

4.2.2 Shear behaviour

The shear strength of the rock-concrete interface and the residual shear strength of the broken interface were determined by shear load tests on cylinders at different constant normal stress levels according to the test programme presented in Table 4-4. For specimens DST-RCI-7 and DST-RCI-8, seven successive shear cycles (s1–s7) were also conducted on the broken interface with various constant normal stress levels. A description of the shear tests can be found in Section 3.3. The specimens were core-drilled from the rock-concrete block 2a, where the concrete was cast on top of a horizontal rock surface. The specimens which were applied with a normal stress had a diameter of 65 mm, whereas the specimens with no applied normal stress had a diameter of 80 mm. The tests were conducted at an age of approximately 90 days.

The shear stress vs. shear displacement from the test on specimens with intact interface are shown in Figure 4-5 and from the tests on broken interface of specimen DST-RCI-7 and DST-RCI-8 are shown in Figure 4-6 and Figure 4-7 respectively. A summary of test results can be found in Table 4-4 and detailed information in Appendix C. The failure of the interface was very brittle resulting in a shear stress drop. In the cases with an applied normal stress, the shear stress drop followed by a new shear stress peak, after which the shear stress declined towards a residual shear stress level of the broken interface. In the tests (DST-RCI-3 and DST-RCI-4) with the highest normal stress level an inclined failure plane crossing the interface was observed, which means that the peak stress and the residual stress are not the exact values of the interface. The friction coefficient μ of the broken interface, determined for each test as the residual shear stress divided by the normal stress, was in the range of 0.60 and 0.86, see Table 4-4. In Figure 4-8 the peak shear stress of the intact interface and the residual shear stress of the broken interface are plotted against the corresponding normal stress.

Table 4-4. Test programme and summary of results for direct shear tests on rock-concrete interface specimens.

Specimen	Area [cm^2]	Age [days]	Shear seq. [1)]	Normal stress [MPa]	Peak shear stress [MPa]	Res. shear stress [MPa]	Res. shear stress/ Normal stress	Failure mode [2)]
DST-RCI-1	32.5	91	s	5	11.5	4.3	0.86	b
DST-RCI-2	32.5	91	s	3	11.0	2.4	0.80	b
DST-RCI-3	32.3	90	s	10	15.6	6.0	0.60	c
DST-RCI-4	32.6	90	s	10	15.7	7.1	0.71	c
DST-RCI-7	50.0	90	s	0	6.1	0	–	a
			s1	5	4.8	4.3	0.85	–
			s2	10	8.5	8.2	0.82	–
			s3	30	23.7	22.4	0.75	–
			s4	20	14.7	14.7	0.74	–
			s5	10	7.8	7.8	0.78	–
			s6	30	21.6	21.6	0.72	–
			s7	5	4.1	4.1	0.81	–
DST-RCI-8	50.6	90	s	0	6.2	0	–	a
			s1	5	3.9	3.5	0.70	–
			s2	10	7.2	7.0	0.70	–
			s3	20	14.1	14.0	0.70	–
			s4	30	20.9	20.8	0.69	–
			s5	20	14.3	14.3	0.72	–
			s6	10	7.4	7.4	0.74	–
			s7	5	3.8	3.8	0.76	–

[1)] Shear sequence: s = shear cycle on intact interface; s# = shear cycle on broken interface.

[2)] Failure mode: a = in interface; b = mainly in interface; c = inclined failure plane crossing interface.

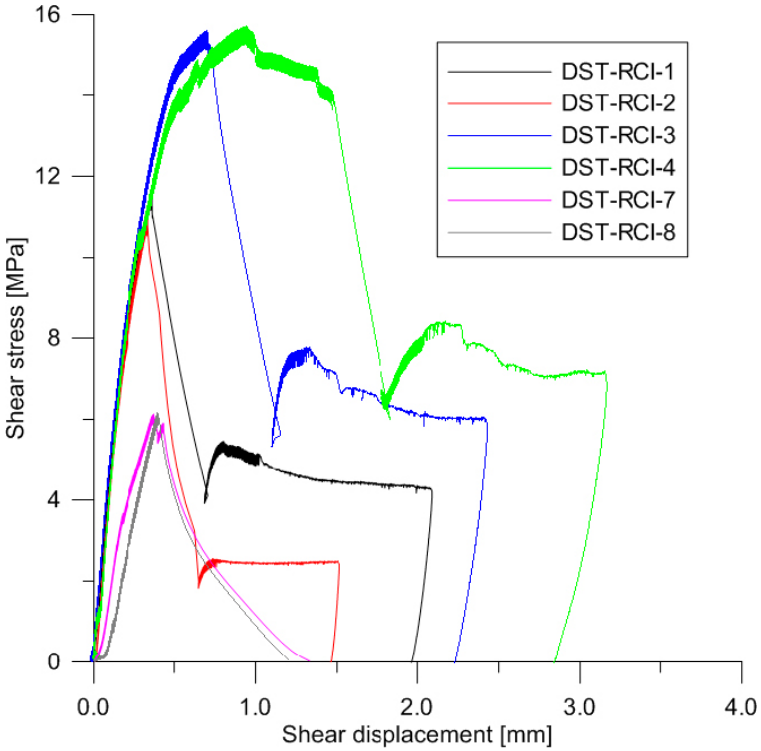

Figure 4-5. *Shear stress vs. shear displacement from direct shear tests on rock-concrete interface specimens (DST-RCI-#).*

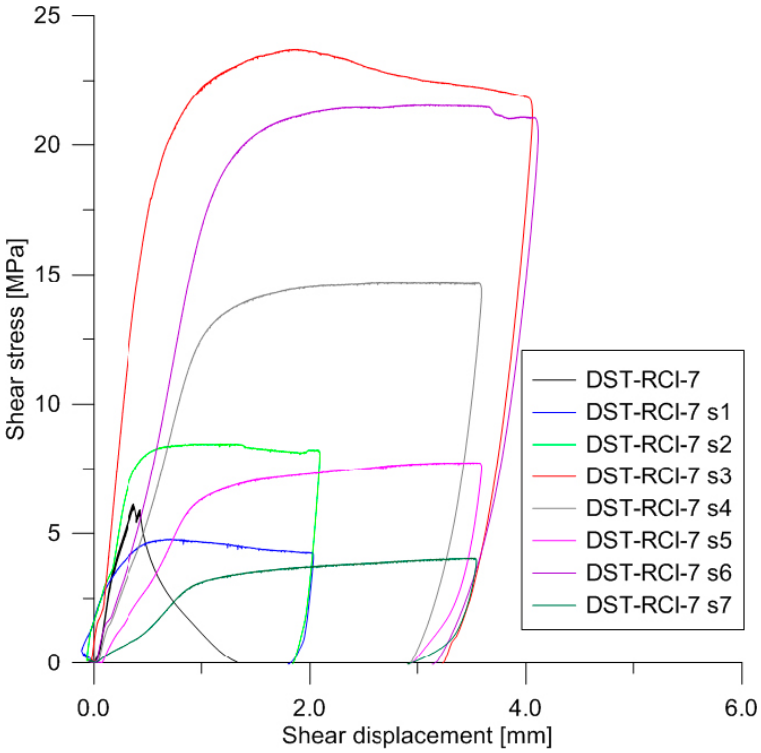

Figure 4-6. *Shear stress vs. shear displacement from direct shear tests on rock-concrete interface specimen DST-RCI-7.*

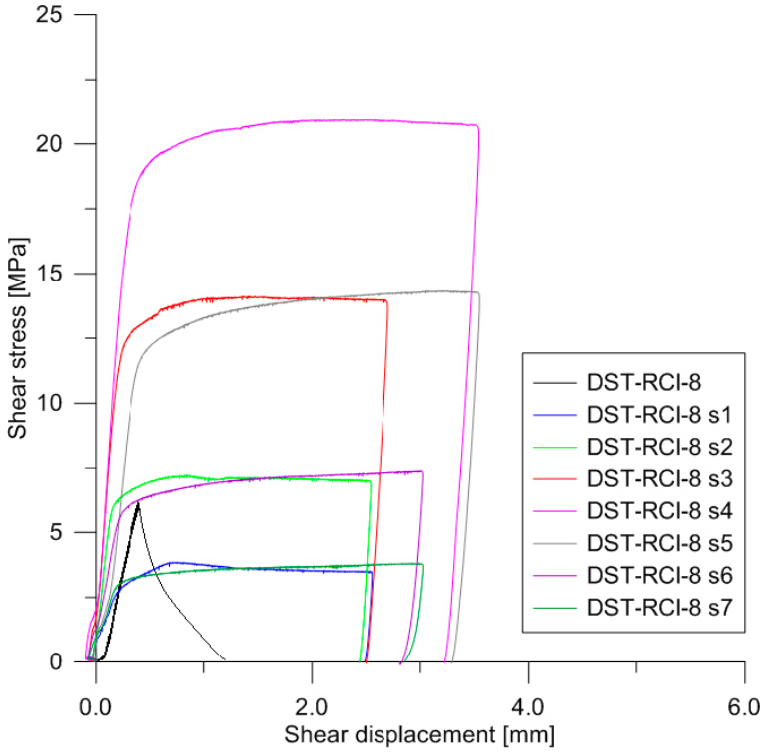

Figure 4-7. *Shear stress vs. shear displacement from direct shear tests on rock-concrete interface specimen DST-RCI-8.*

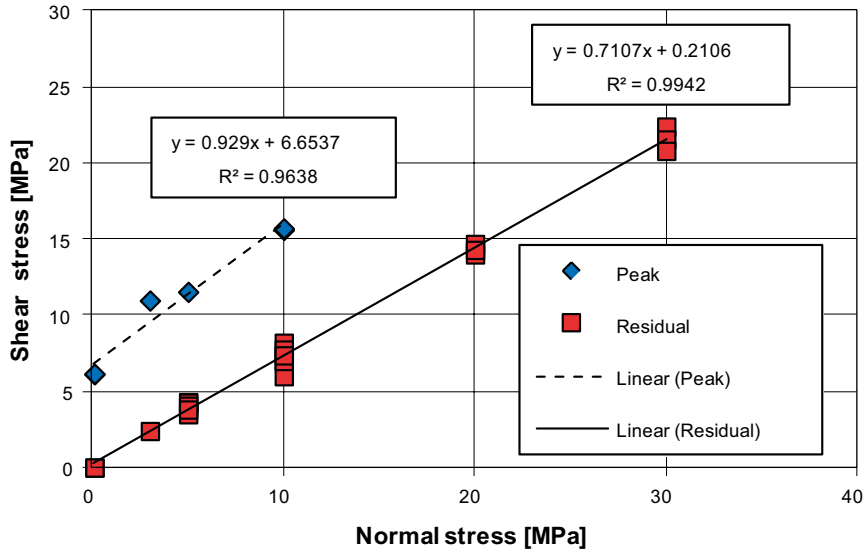

Figure 4-8. *Peak shear stress and residual shear stress vs. normal stress from direct shear tests on rock-concrete interface specimens.*

5 Conclusions

In this study, the mechanical properties of the interface between the low-pH concrete B200 and the wire sawn rock surface are investigated. The mechanical testing of the rock-concrete interface is conducted on cylinders, which are core-drilled from rock-concrete blocks. The blocks are manufactured by casting concrete against the wire sawn surfaces of rock panels from the Äspö Hard Rock Laboratory.

The following mechanical properties of the concrete material are evaluated: the compressive strength, the splitting tensile strength, the direct tensile strength and the fracture energy.

The tensile bond strength is determined by pull-off tests on cylinders cored through the rock-concrete interface at different times after casting. A significant difference in bond strength between vertical interface and horizontal interface is observed (see Figure 5-1). For the specimens taken from blocks with vertical interface the majority of the failures occur at the interface, while for the specimens taken from blocks with horizontal interface the majority of the failures occur instead in the concrete. The lower bond strength together with the interface failures suggest that the bond is weaker when the concrete is cast against a vertical rock surface.

The tensile softening behaviour of the interface is also evaluated 90 days after casting from direct tensile tests on rock-concrete cores drilled from a panel with horizontal interface. The crack propagation is registered during the testing by the use of an optical full-field deformation measurement system. The tensile bond strength measured is at the same level as the tensile strength of the concrete. The fracture energy from the rock-concrete interface cracking is found to be about 1/5 of the concrete fracture energy.

The shear strength of the rock-concrete interface and the residual shear strength of the broken interface are determined by shear load tests at different constant normal stress levels on cylinders core-drilled from a rock-concrete block. The friction coefficient μ of the broken interface, determined for each test as the residual shear stress divided by the normal stress, is in the range of 0.60 and 0.86.

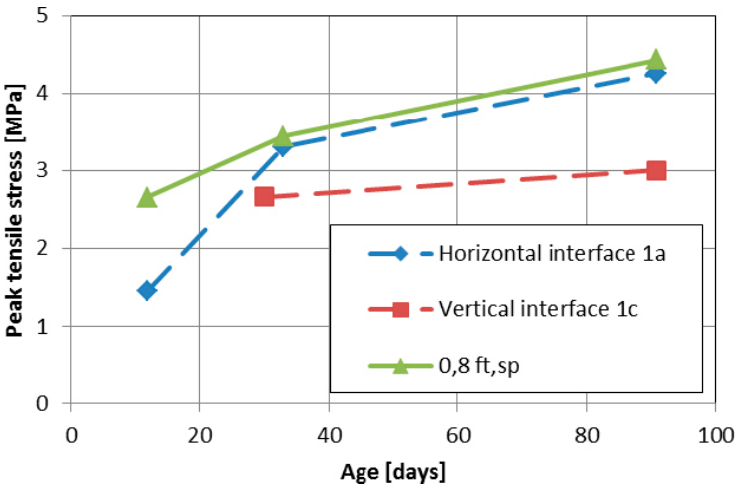

Figure 5-1. *Development of peak tensile stress at the rock-concrete interface and tensile strength of the concrete (assumed as 80% of the splitting tensile strength).*

References

SKB's (Svensk Kärnbränslehantering AB) publications can be found at www.skb.se/publications.

RILEM, 2001. RILEM TC 162-TDF: Uni-axial tension test for steel fibre reinforced concrete. Materials and Structures 34, 3–6.

RILEM, 2007. Experimental determination of the stress-crack opening curve for concrete in tension. Report 39 RILEM TC 187-SOC, RILEM, France.

SS 137231:2005. Concrete testing – Hardened concrete – tensile strength of test specimens. Stockholm: Swedish Standards Institute.

SS-EN 12390-3:2009. Testing hardened concrete – Part 3: Compressive strength of test specimens. Stockholm: Swedish Standards Institute.

SS-EN 12390-6:2009. Testing hardened concrete – Part 6: Tensile splitting strength of test specimens. Stockholm: Swedish Standards Institute.

SS-EN 12504-1:2009. Testing concrete in structures – Part 1: Cored specimens – Taking, examination and testing in compression. Stockholm: Swedish Standards Institute.

Vogt C, Lagerblad B, Wallin K, Baldy F, Jonasson J-E, 2009. Low pH self compacting concrete for deposition tunnel plugs. SKB R-09-07, Svensk Kärnbränslehantering AB.

Appendix A

Characteristics of the wire sawn rock surfaces

The characteristics of the wire sawn surfaces were documented with optical 3D-scanning as described in Section 2.1. This appendix contains results from the measurements of the rock surfaces 1a, 1c and 2a (Figures A-1 to A-3) that were used in the tests reported in Section 4. An average plane was adapted to the considered surface and the surface deviation was calculated with respect to that plane. For each surface, the surface deviation was evaluated both for an area of approximately 550×350 mm^2 and for a close up area of approximately 100×100 mm^2; see Figures A-4 to A-9. As a measurement of the surface roughness, the arithmetic average value S_A of the surface deviation from the average plane of the close up area was calculated. The S_A-value was 0.09 mm for 1a, 0.16 mm for 1c and 0.12 mm for 2a.

Figure A-1. *Photo of the wire sawn rock surface 1a.*

Figure A-2. *Photo of the wire sawn rock surface 1c.*

Figure A-3. *Photo of the wire sawn rock surface 2a.*

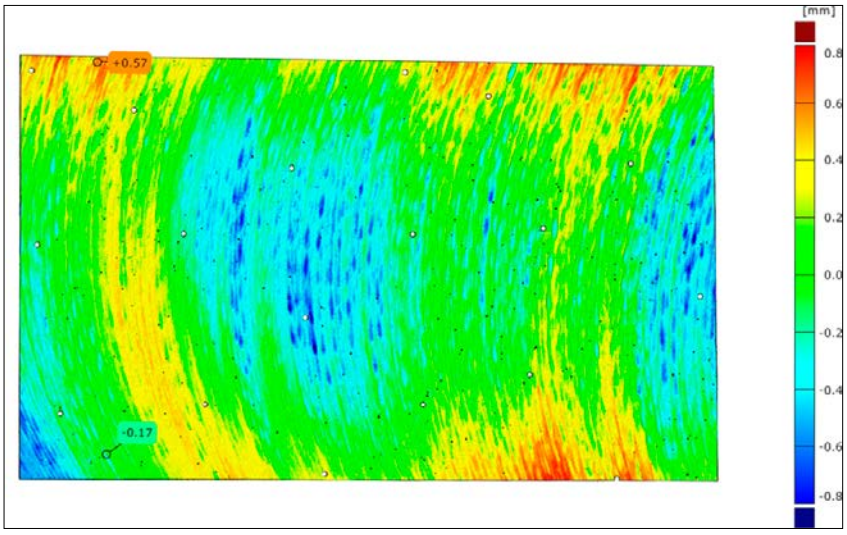

Figure A-4. *Contour plot of the surface deviation from the mean plane of the wire sawn rock surface 1a.*

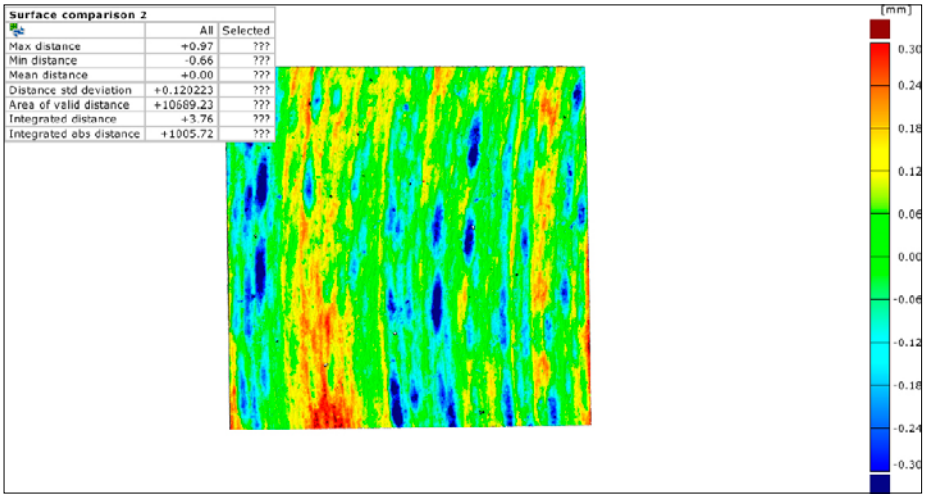

Figure A-5. *Contour plot of the surface deviation from the mean plane of 100x100 mm2 of the wire sawn rock surface 1a.*

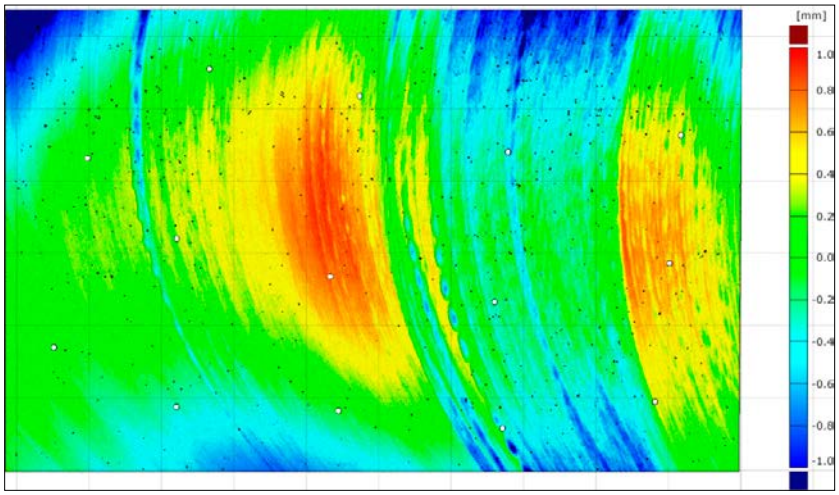

Figure A-6. *Contour plot of the surface deviation from the mean plane of the wire sawn rock surface 1c.*

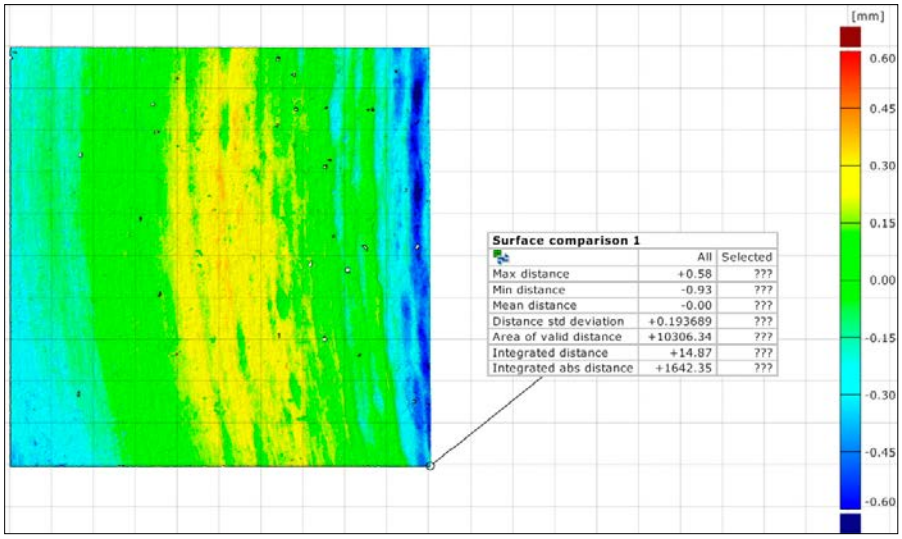

Figure A-7. *Contour plot of the surface deviation from the mean plane of 100x100 mm^2 of the wire sawn rock surface 1c.*

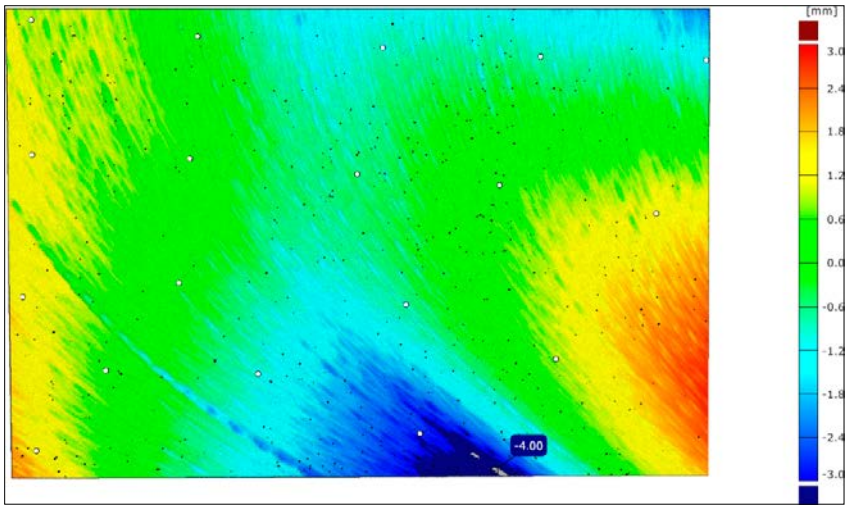

Figure A-8. *Contour plot of the surface deviation from the mean plane of the wire sawn rock surface 2a.*

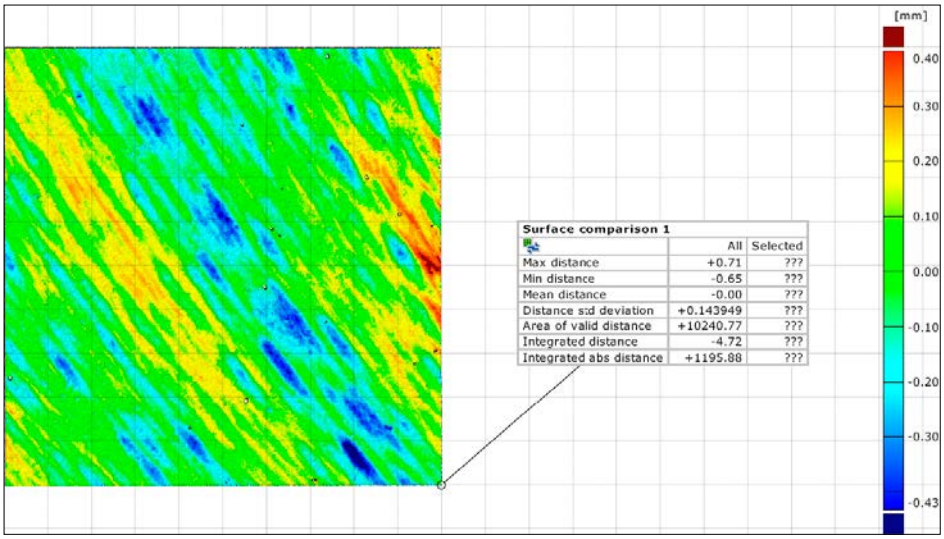

Figure A-9. *Contour plot of the surface deviation from the mean plane of 100x100 mm^2 of the wire sawn rock surface 2a.*

Appendix B

Summary of concrete material test results

This appendix summarises the results of the concrete material tests presented in Section 4.1. The evaluated concrete material properties are presented in Table B-1 to B-6. The tensile stress-displacement relations from the direct tensile tests are shown in Figure B-1 to B-6. Photo of the direct tensile test specimens after testing is shown in Figure B-7.

Table B-1. Compressive strength at 90 days – 150 mm cube.

Specimen #	Density, ρ [kg/m^3]	$f_{c,cube}$ [MPa]
1	2370	81.6
2	2370	84.4
3	2380	82.7
4	2370	82.2
5	2380	78.5
Mean	*2374*	*81.9*
Std. dev.	*5.5*	*2.2*

Table B-2. Compressive strength at 90 days – Ø150×300 mm cylinder.

Specimen #	Density, ρ [kg/m^3]	$f_{c,cyl}$ [MPa]
1	2350	79.0
2	2350	78.0
3	2330	77.4
4	2340	77.6
5	2340	78.0
Mean	*2342*	*78.0*
Std. dev.	*8.4*	*0.6*

Table B-3. Compressive strength – core specimens Ø100×100 mm.

Specimen #	12 days ρ [kg/m^3]	f_c [MPa]	29 days ρ [kg/m^3]	f_c [MPa]	90 days ρ [kg/m^3]	f_c [MPa]
1	2310	33.3	2320	56.4	2320	82.0
2	2320	34.6	2330	54.5	2330	81.1
3	2310	33.4	2330	55.3	2340	83.9
4	2300	33.4	2320	54.0	2330	81.0
5	2310	33.6	2330	55.2	2340	82.9
Mean	*2310*	*33.7*	*2326*	*55.1*	*2332*	*82.2*
Std. dev.	*7.1*	*0.5*	*5.5*	*0.9*	*8.4*	*1.2*

Table B-4. Splitting tensile strength – core specimens Ø100×100 mm. Measured density ρ (kg/m^3) is given in brackets.

Specimen #	$f_{ct,sp}$ [MPa] 12 days	29 days	90 days
1	3.2 (2320)	4.4 (2340)	5.2 (2330)
2	3.1 (2320)	4.5 (2350)	5.3 (2340)
3	3.5 (2310)	3.9 (2340)	6.0 (2350)
4	3.4 (2320)	4.0 (2340)	5.3 (2350)
5	3.4 (2310)	4.7 (2360)	5.9 (2350)
Mean	***3.3***	***4.3***	***5.5***
Std. dev.	***0.2***	***0.3***	***0.4***

Table B-5. Tensile strength at 90 days – core specimens Ø65×100 mm.

Specimen #	f_{ctm} [MPa]
1	3.4
2	3.1
3	2.7
4	3.2
5	3.0
6	3.8
Mean	***3.2***
Std. dev.	***0.4***

Table B-6. Tensile strength and fracture energy – notched core specimens Ø100×100 mm.

Specimen	Area [cm^2]	Age [days]	f_{ctm} [MPa]	G_F [N/m]
DTT-C-2	50.9	89	3.8	109
DTT-C-3	49.4	89	3.6	111
DTT-C-4	49.6	90	3.6	127
DTT-C-5	49.9	90	3.6	146
DTT-C-6	49.5	90	3.9	106
DTT-C-7	49.5	90	3.3	129
		Mean	***3.6***	***121***
		Std. dev.	***0.2***	***15***

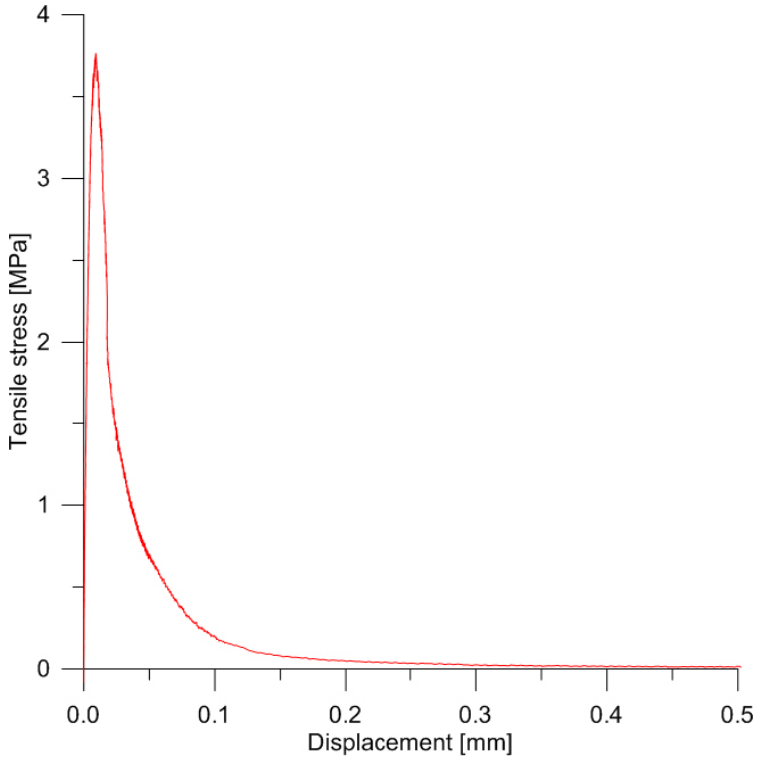

Figure B-1. *Tensile stress vs displacement for specimen DTT-C-2.*

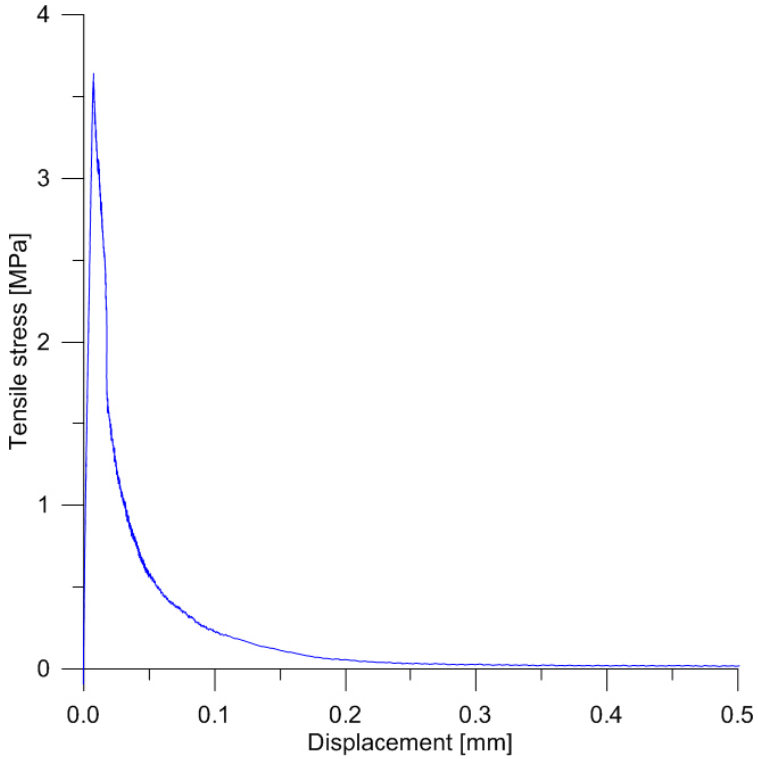

Figure B-2. *Tensile stress vs displacement for specimen DTT-C-3.*

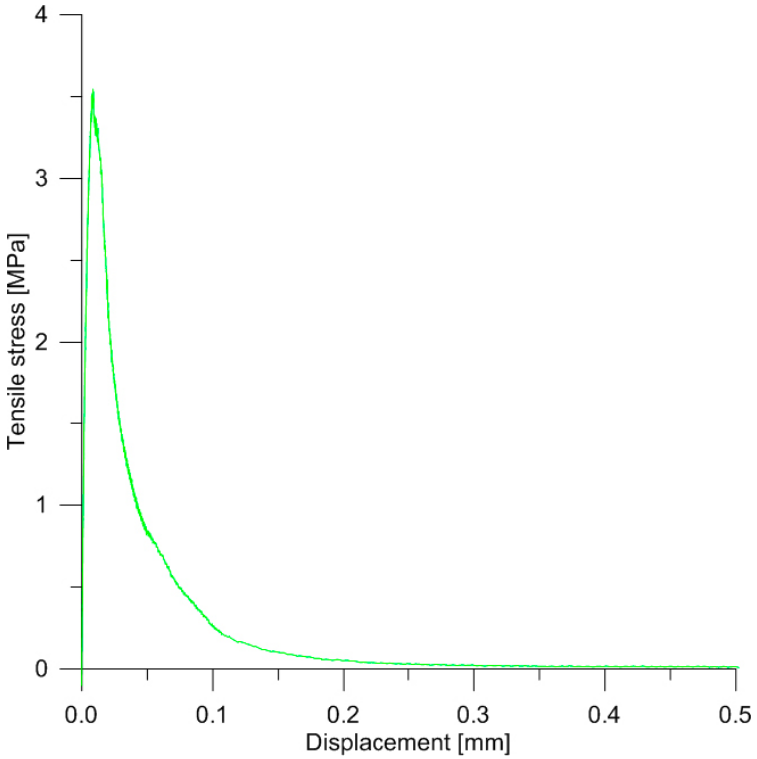

Figure B-3. *Tensile stress vs displacement for specimen DTT-C-4.*

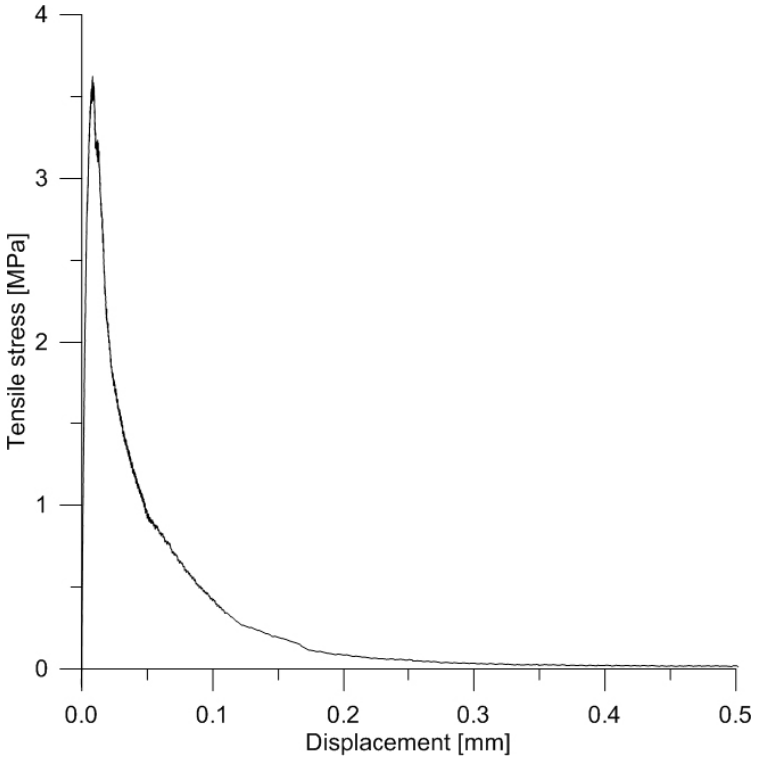

Figure B-4. *Tensile stress vs displacement for specimen DTT-C-5.*

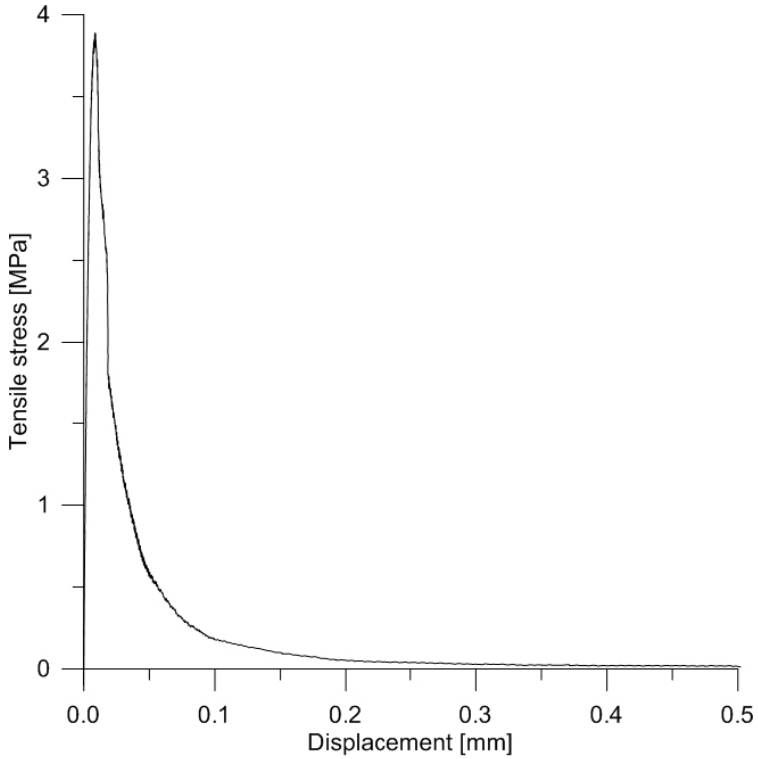

Figure B-5. *Tensile stress vs displacement for specimen DTT-C-6.*

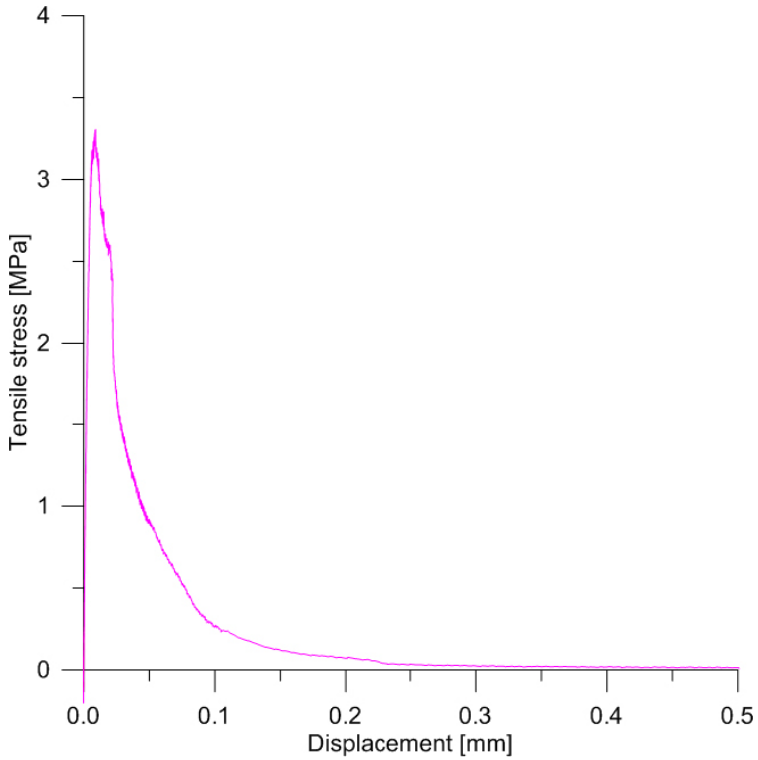

Figure B-6. *Tensile stress vs displacement for specimen DTT-C-7.*

Figure B-7. *Photo of the direct tensile tests specimens (DTT-C-#) after testing.*

Appendix C

Summary of rock-concrete interface test results

This appendix summarises the results of the mechanical testing of the rock-concrete interface presented in Section 4.2. The tensile bond strength determined at different ages by pull-off tests are summarized in Table C-1 to C-6. The tensile stress-displacement relations, together with results from the optical full-field deformation measurements, from the direct tensile tests are shown in Figure C-1 to C-6 and the shear stress-shear displacement relations from the direct shear tests are shown in Figure C-8 to C-27. Photos of the specimens after testing can be found in Figures C7 and C28 to C33.

Tensile bond strength

Table C-1. Tensile bond strength for horizontal interface 1a at the age of 12 days.

Specimen #	Age [days]	Failure mode	Distance from surface [mm]	Peak tensile stress [MPa]	Tensile bond strength [MPa]
1	12	Interface		1.48	1.48
2	12	Concrete	1–2	1.47	–
3	12	Interface [1)]		–	–
4	12	Interface [1)]		–	–
5	12	Concrete	1–2	1.40	–
6	12	Concrete	1–2	1.47	–
7	12	Interface [1)]		–	–
			Mean	***1.45***	***1.48***
			Std. dev.	***0.04***	

[1)] Interface failure at drilling.

Table C-2. Tensile bond strength for horizontal interface 1a at the age of 33 days.

Specimen #	Age [days]	Failure mode	Distance from surface [mm]	Peak tensile stress [MPa]	Tensile bond strength [MPa]
2	33	Interface		3.53	3.53
5	33	Interface		3.27	3.27
6	33	Concrete	3–4	3.27	–
8	33	Interface		3.32	3.32
9	33	Concrete	10–13	3.09	–
10	33	Concrete	70–75	3.95	–
11	33	Concrete	1–4	3.26	–
12	33	Concrete	2–3	3.00	–
13	33	Concrete	1–2	3.06	–
			Mean	***3.31***	***3.37***
			Std. dev.	***0.29***	***0.14***

Table C-3. Tensile bond strength for horizontal interface 1a at the age of 91 days.

Specimen #	Age [days]	Failure mode	Distance from surface [mm]	Peak tensile stress [MPa]	Tensile bond strength [MPa]
1	91	Concrete	10	3.85	–
2	91	Interface		4.28	4.28
3	91	Concrete	35	4.43	–
4	91	Interface		4.75	4.75
5	91	Interface		4.41	4.41
6	91	Concrete	90	4.14	–
7	91	Concrete	20–30	4.23	–
8	91	Concrete	10	4.22	–
9	91	Concrete	20	4.24	–
10	91	Concrete	10	4.16	–
11	91	Interface		4.10	4.10
			Mean	***4.25***	***4.38***
			Std. dev.	***0.23***	***0.28***

Table C-4. Tensile bond strength for vertical interface 1c at the age of 12 days.

Specimen #	Age [days]	Failure mode	Distance from surface [mm]	Peak tensile stress [MPa]	Tensile bond strength [MPa]
1	12	Interface [1)]		–	–
2	12	Interface [1)]		–	–
6	12	Interface [1)]		–	–
			Mean	**–**	**–**
			Std. dev.	**–**	**–**

[1)] Interface failure at drilling.

Table C-5. Tensile bond strength for vertical interface 1c at the age of 30 days.

Specimen #	Age [days]	Failure mode	Distance from surface [mm]	Peak tensile stress [MPa]	Tensile bond strength [MPa]
3	30	Concrete	1–2	3.26	–
4	30	Interface		2.41	2.41
5	30	Interface		2.63	2.63
7	30	Interface [1)]		–	–
8	30	Interface [1)]		–	–
9	30	Interface		1.88	1.88
10	30	Interface [1)]		–	–
11	30	Interface		3.11	3.11
			Mean	***2.66***	***2.51***
			Std. dev.	***0.55***	***0.51***

[1)] Interface failure at drilling.

Table C-6. Tensile bond strength for vertical interface 1c at the age of 91 days.

Specimen #	Age [days]	Failure mode	Distance from surface [mm]	Peak tensile stress [MPa]	Tensile bond strength [MPa]
1	91	Interface		2.45	2.45
4	91	Interface		2.22	2.22
5	91	Interface		3.10	3.10
6	91	Concrete	5–10	3.70	–
7	91	Interface		3.12	3.12
8	91	Interface		3.38	3.38
9	91	Interface		3.16	3.16
10	91	Interface		2.90	2.90
11	91	Interface [1)]		–	–
12	91	Interface [1)]		–	–
13	91	Interface [1)]		–	–
			Mean	***3.00***	***2.90***
			Std. dev.	***0.48***	***0.42***

[1)] Interface failure at drilling.

Direct tensile tests

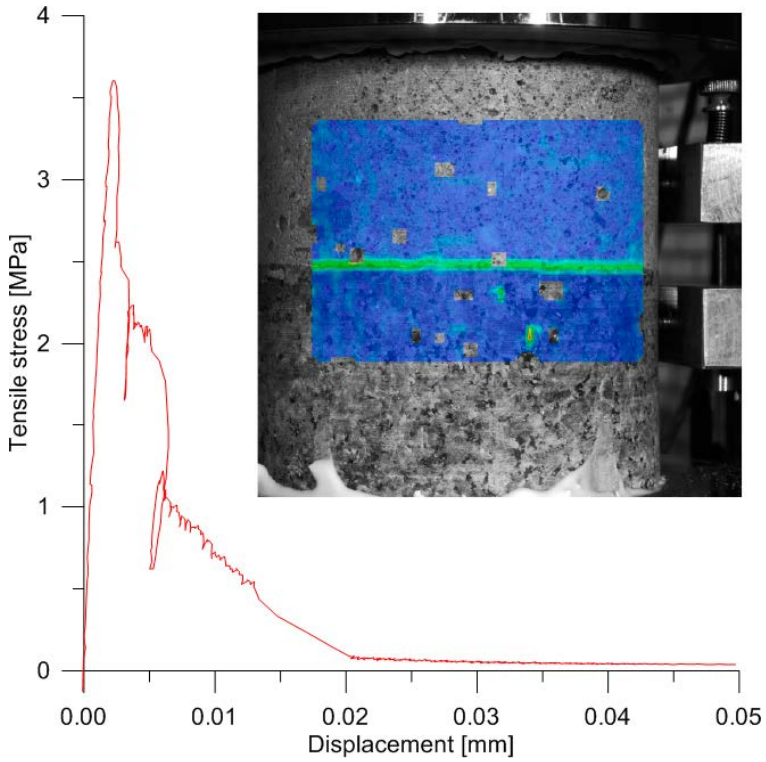

Figure C-1. *Tensile stress vs displacement for specimen DTT-RCI-2.*

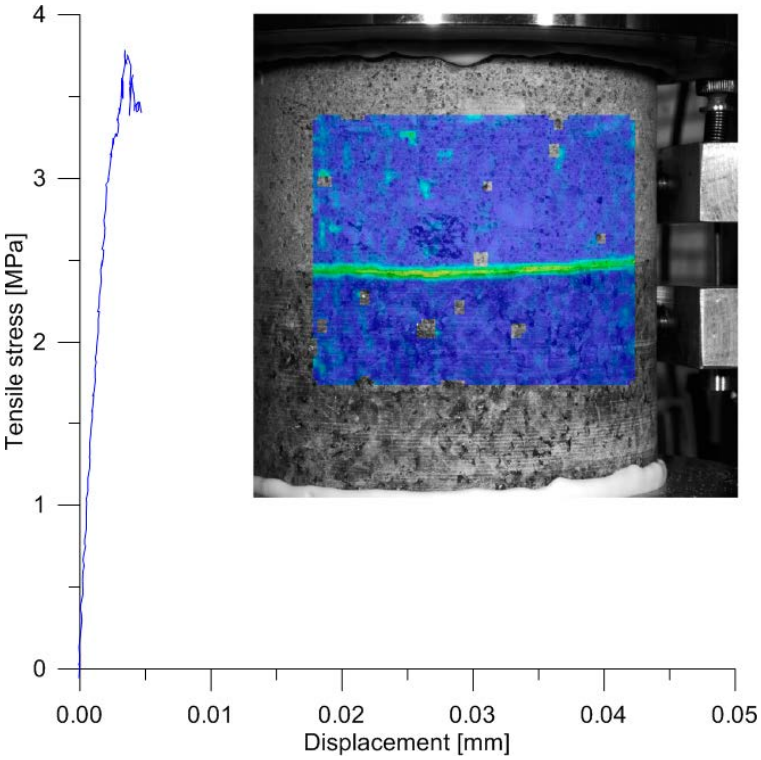

Figure C-2. *Tensile stress vs displacement for specimen DTT-RCI-3.*

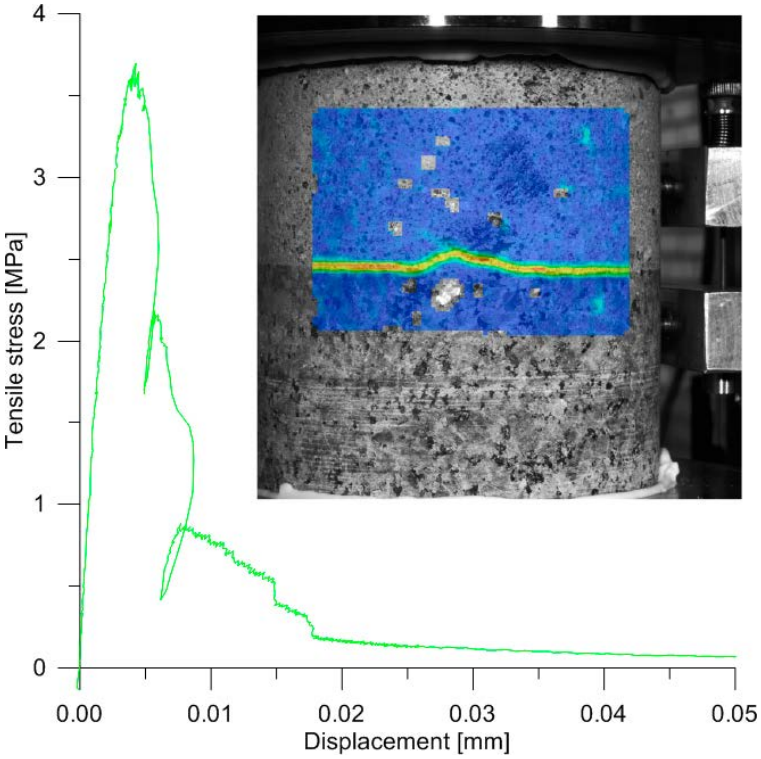

Figure C-3. *Tensile stress vs displacement for specimen DTT-RCI-4.*

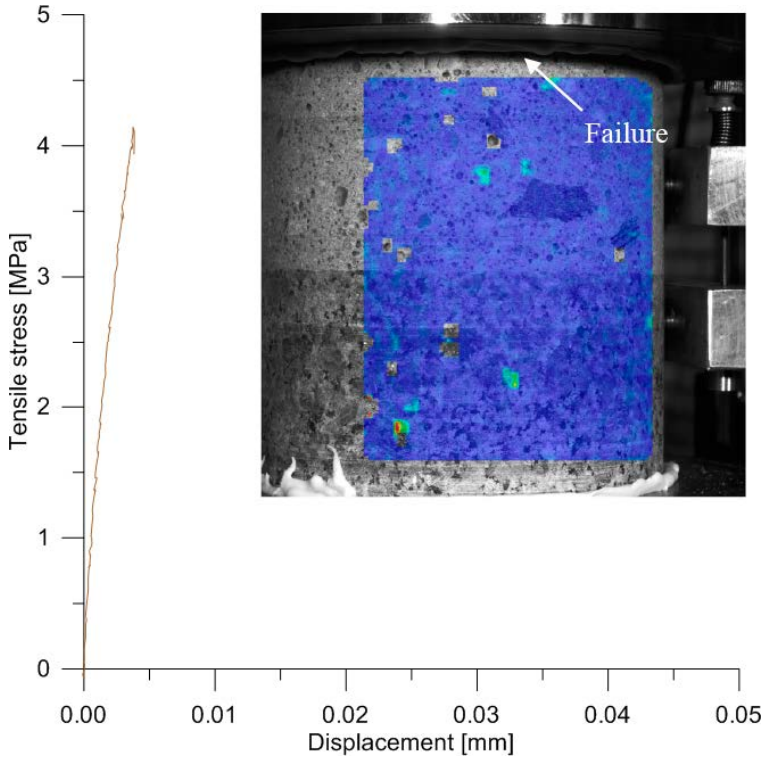

Figure C-4. *Tensile stress vs displacement for specimen DTT-RCI-5.*

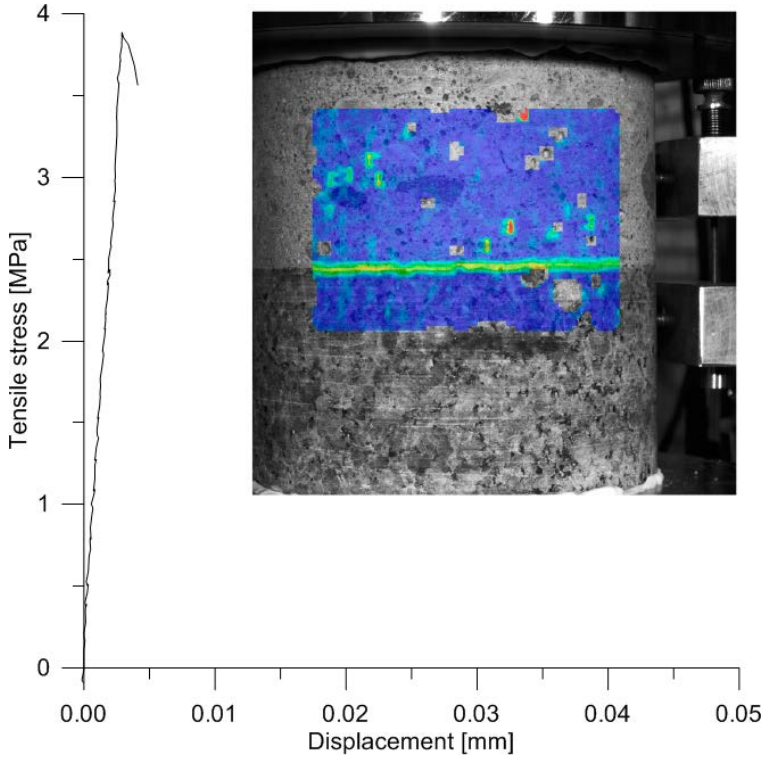

Figure C-5. *Tensile stress vs displacement for specimen DTT-RCI-6.*

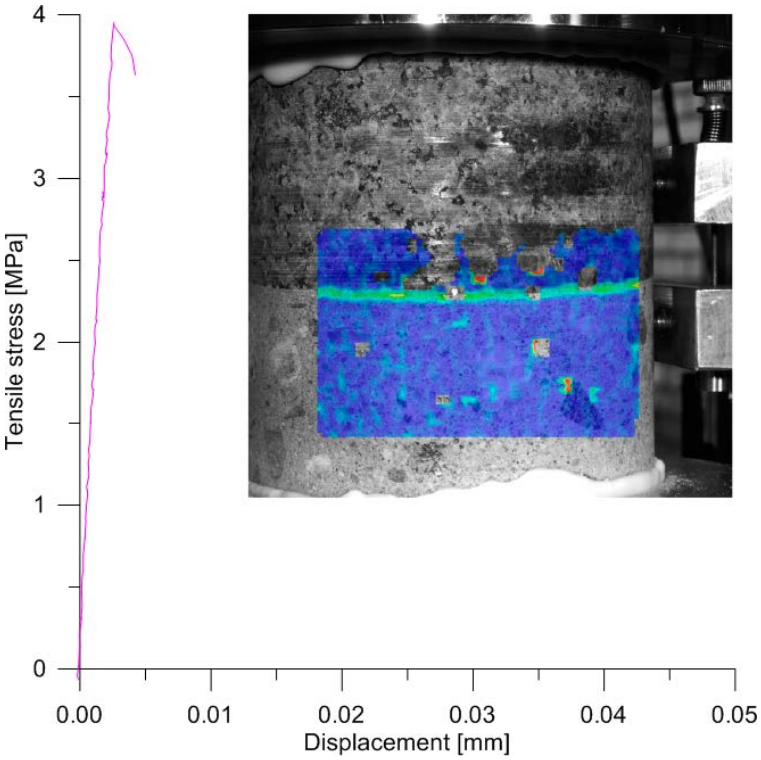

Figure C-6. *Tensile stress vs displacement for specimen DTT-RCI-7.*

Figure C-7. *Photo of the direct tensile tests on rock-concrete interface specimens (DTT-RCI-#) after testing.*

Direct shear tests

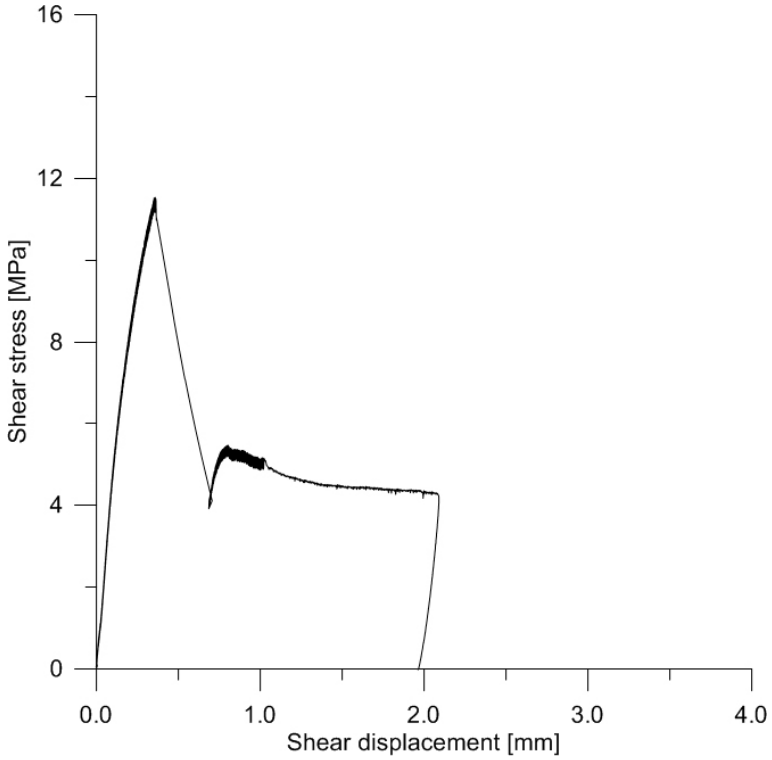

Figure C-8. *Shear stress vs. shear displacement for specimen DST-RCI-1.*

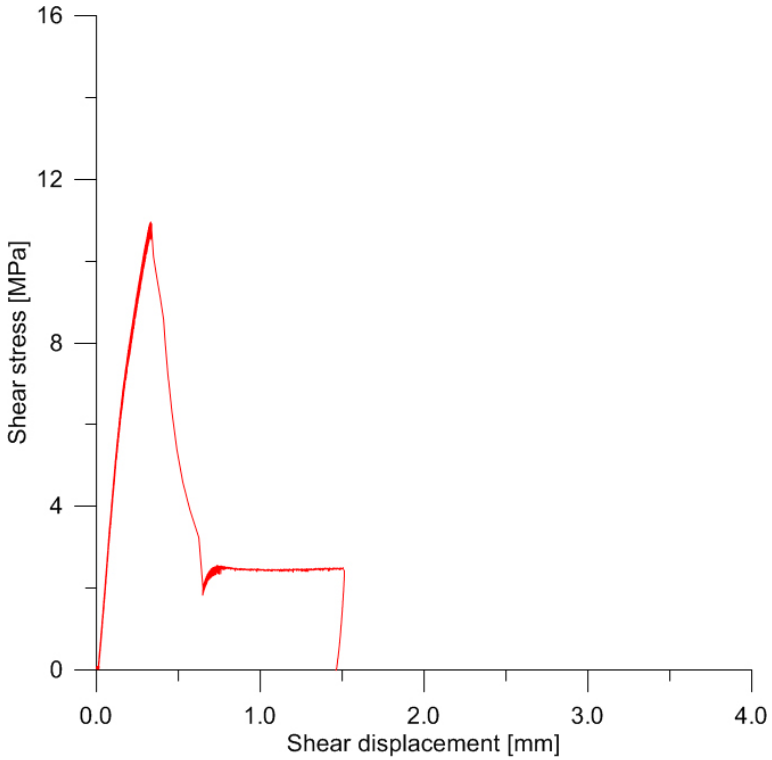

Figure C-9. *Shear stress vs. shear displacement for specimen DST-RCI-2.*

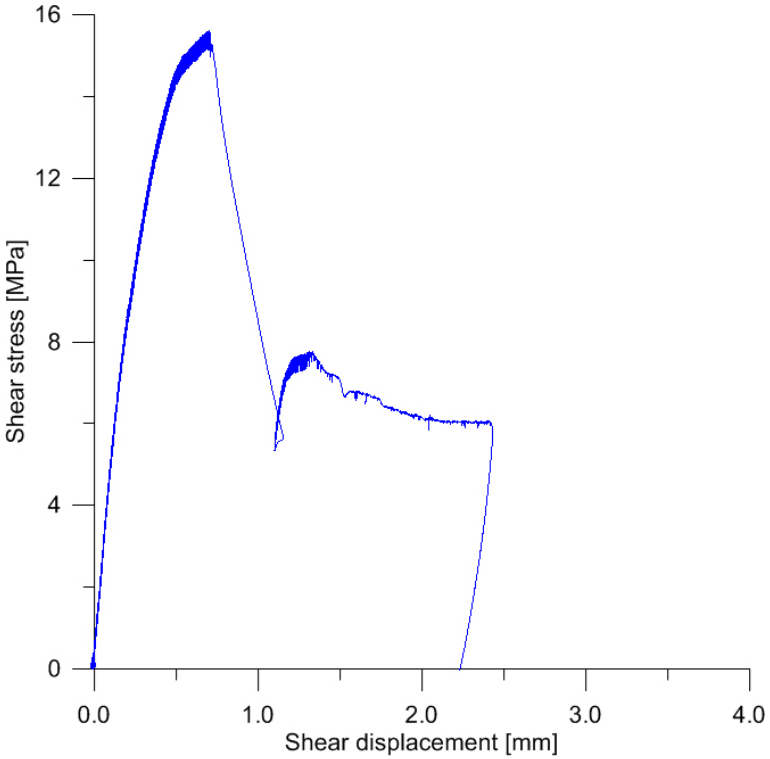

Figure C-10. *Shear stress vs. shear displacement for specimen DST-RCI-3.*

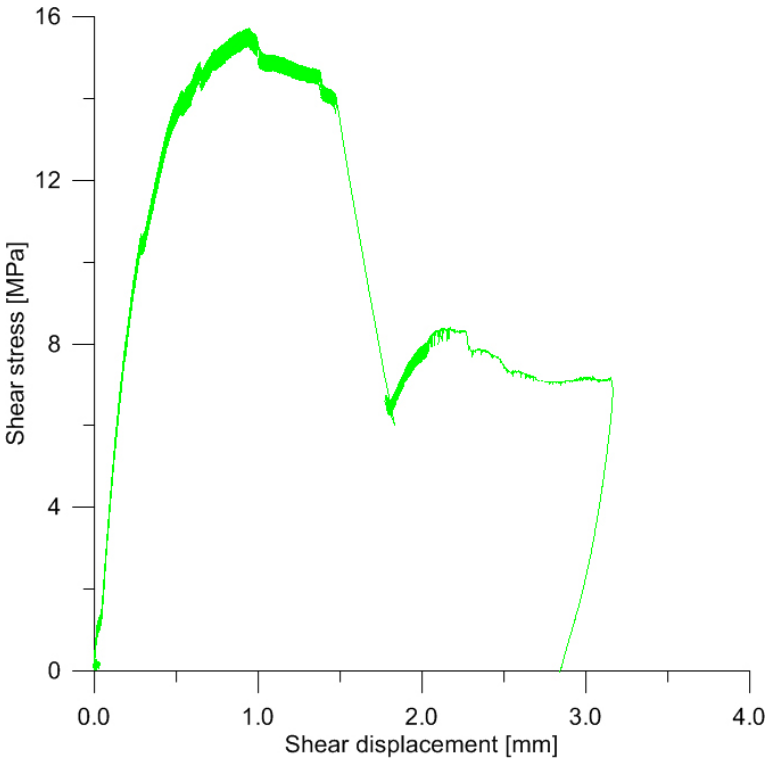

Figure C-11. *Shear stress vs. shear displacement for specimen DST-RCI-4.*

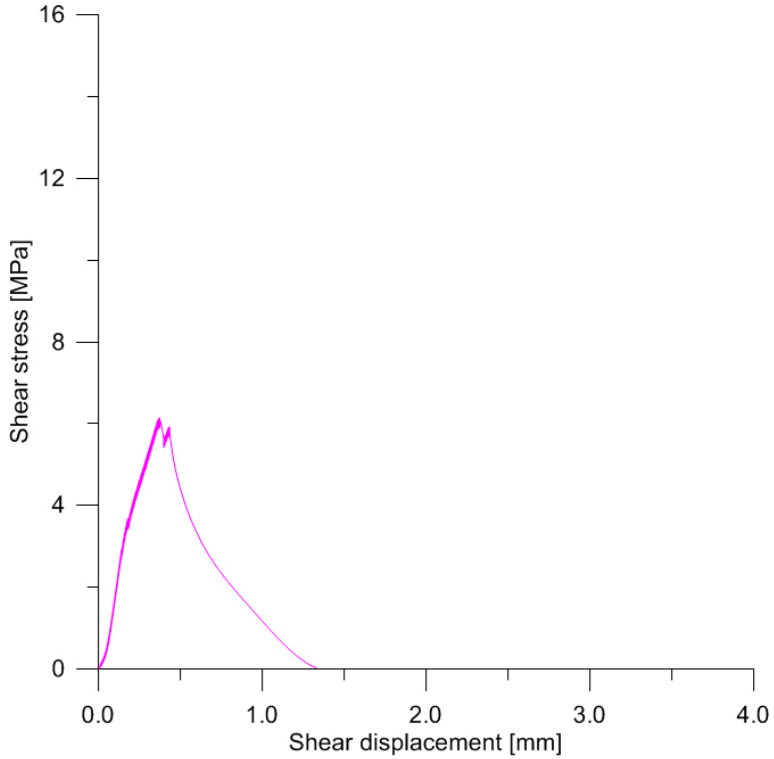

Figure C-12. *Shear stress vs. shear displacement for specimen DST-RCI-7.*

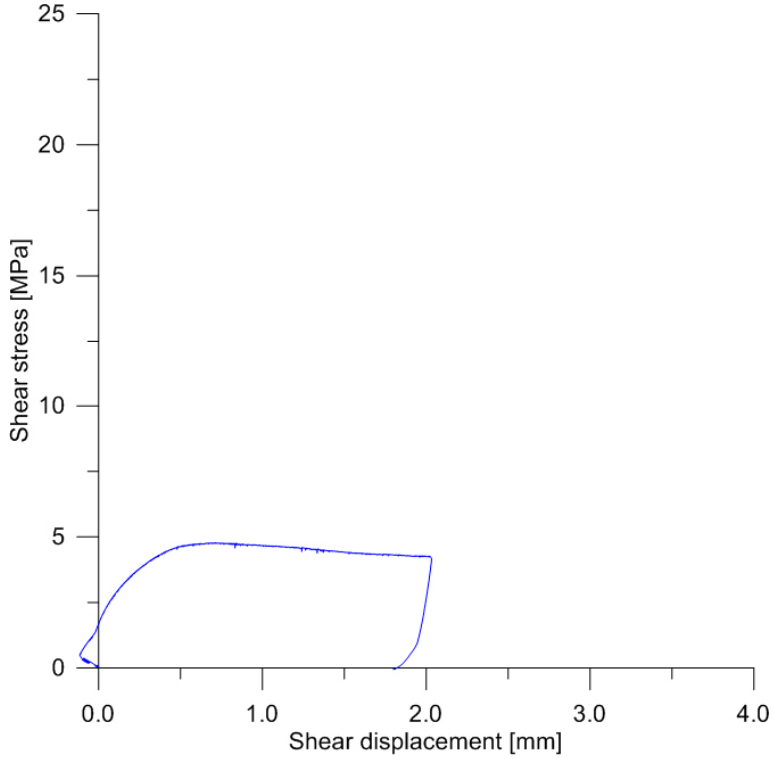

Figure C-13. *Shear stress vs. shear displacement for specimen DST-RCI-7 shear cycle s1.*

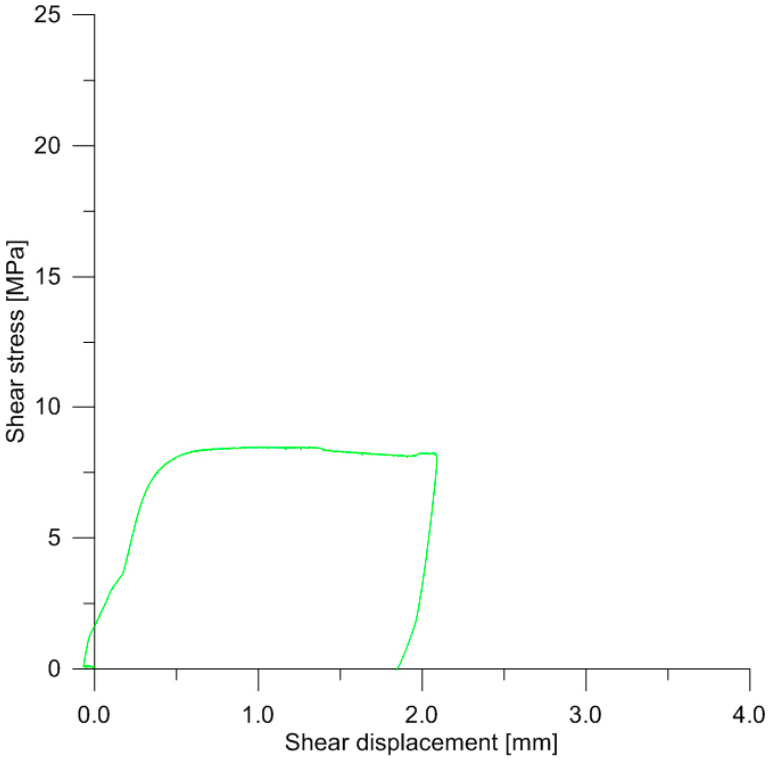

Figure C-14. *Shear stress vs. shear displacement for specimen DST-RCI-7 shear cycle s2.*

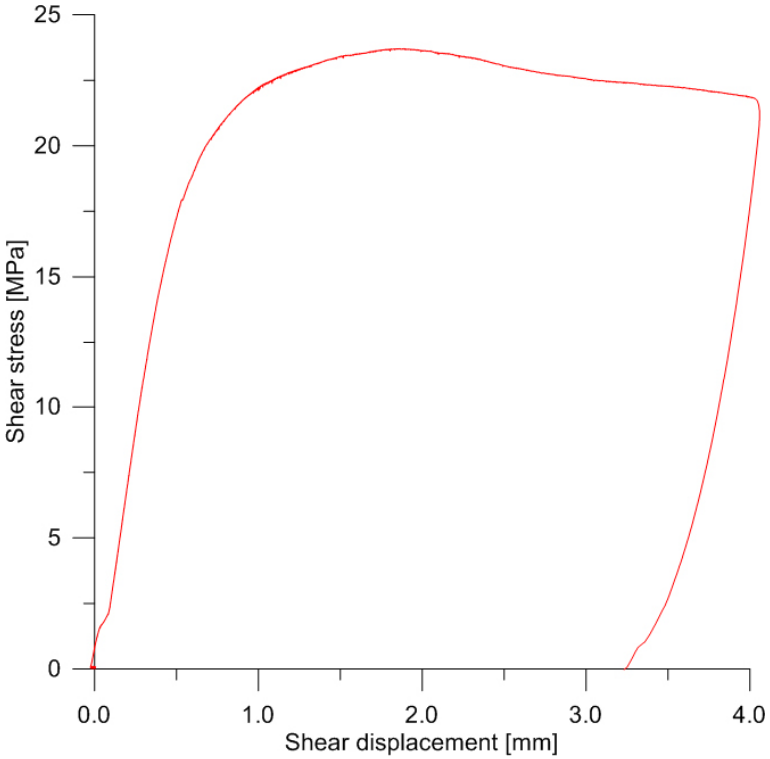

Figure C-15. *Shear stress vs. shear displacement for specimen DST-RCI-7 shear cycle s3.*

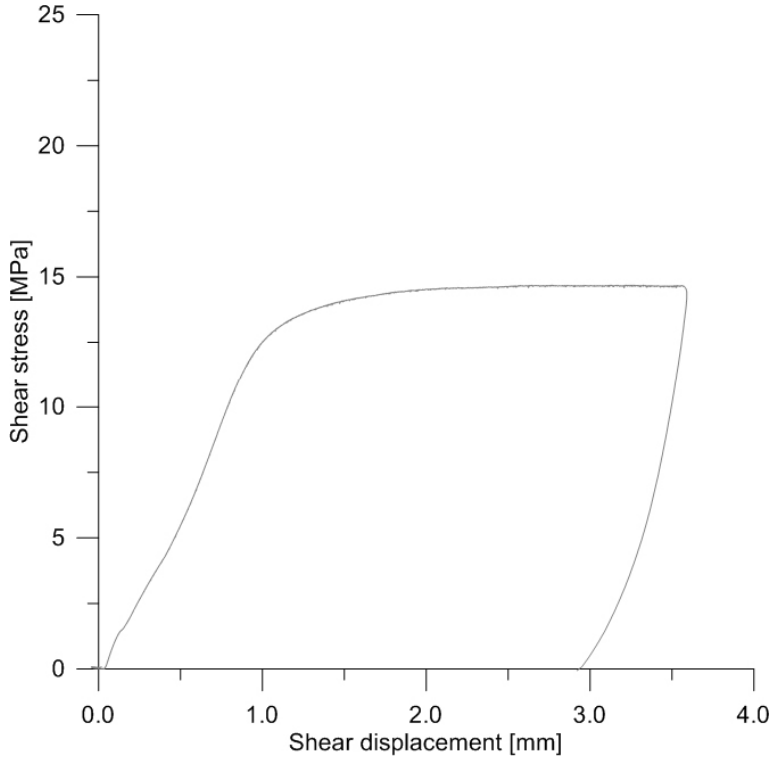

Figure C-16. *Shear stress vs. shear displacement for specimen DST-RCI-7 shear cycle s4.*

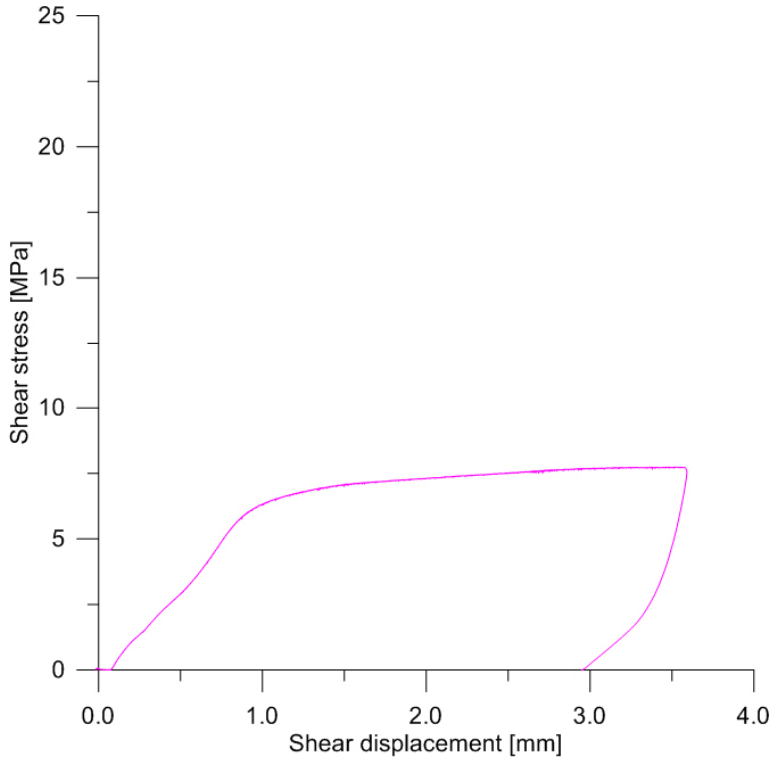

Figure C-17. *Shear stress vs. shear displacement for specimen DST-RCI-7 shear cycle s5.*

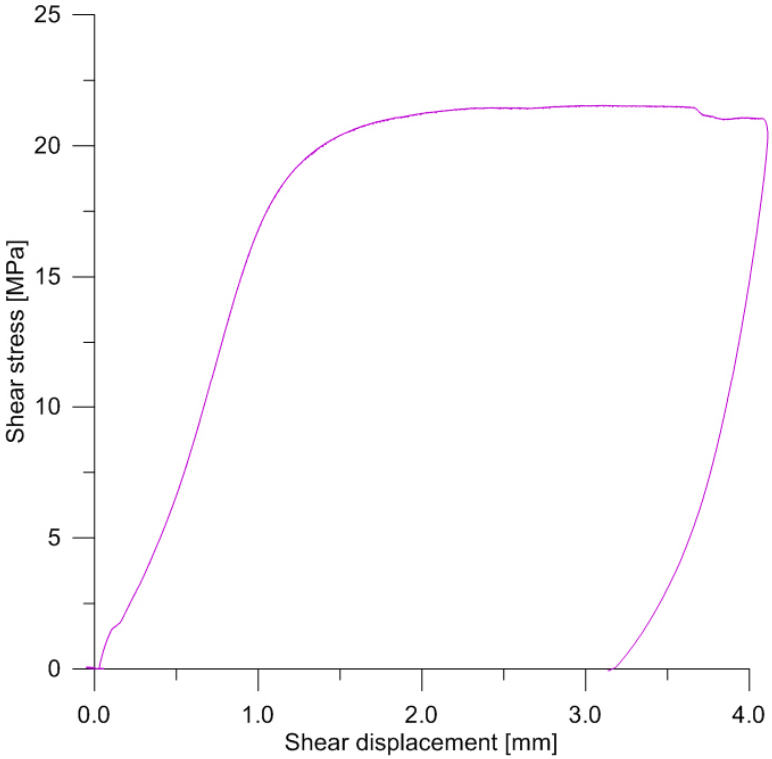

Figure C-18. *Shear stress vs. shear displacement for specimen DST-RCI-7 shear cycle s6.*

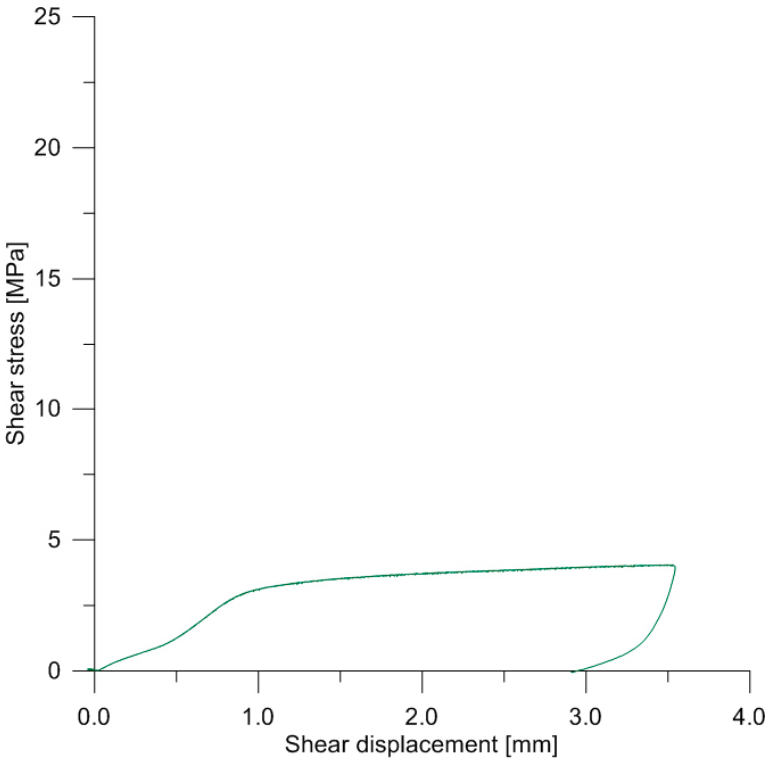

Figure C-19. *Shear stress vs. shear displacement for specimen DST-RCI-7 shear cycle s7.*

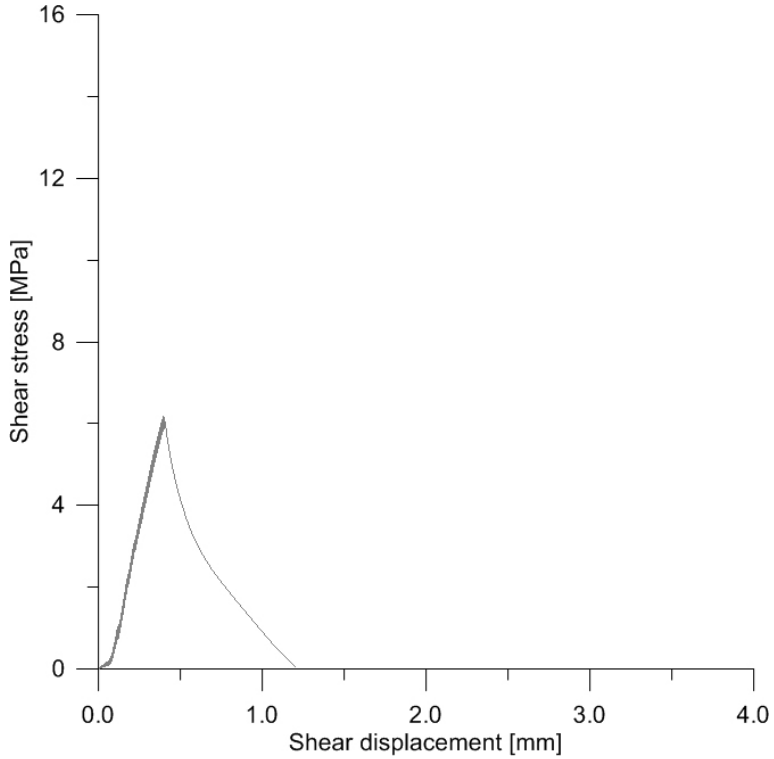

Figure C-20. *Shear stress vs. shear displacement for specimen DST-RCI-8.*

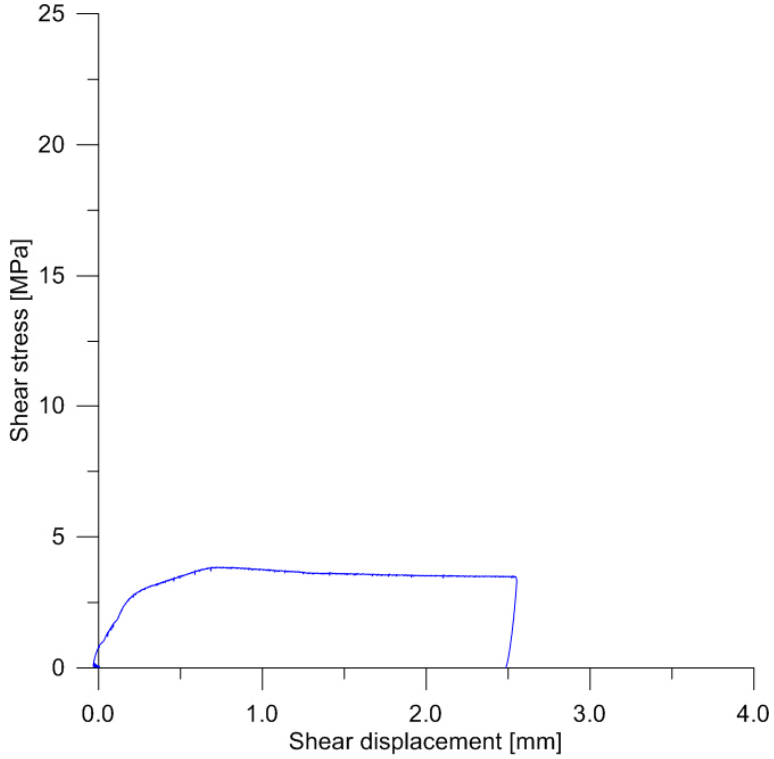

Figure C-21. *Shear stress vs. shear displacement for specimen DST-RCI-8 shear cycle s1.*

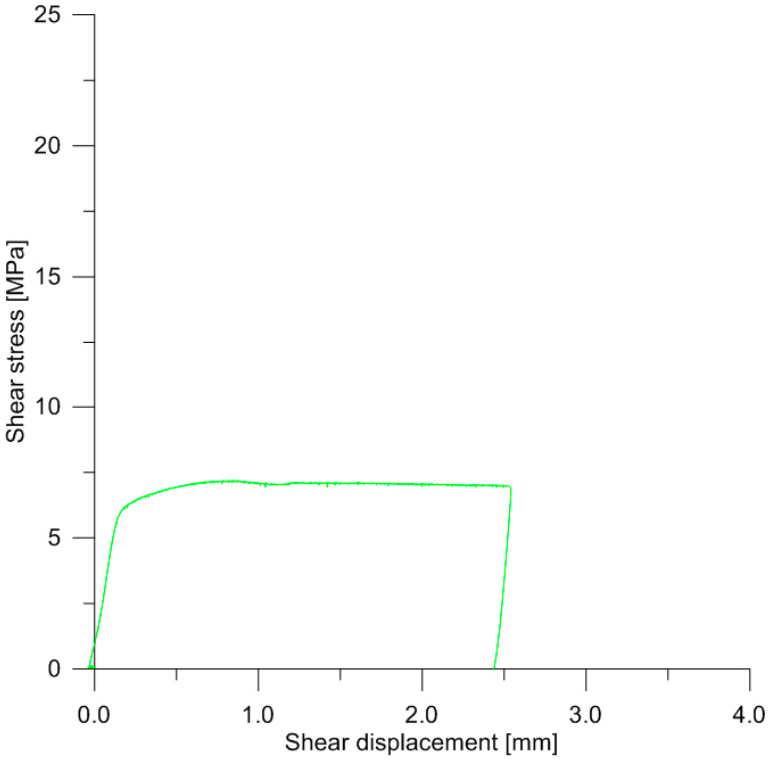

Figure C-22. *Shear stress vs. shear displacement for specimen DST-RCI-8 shear cycle s2.*

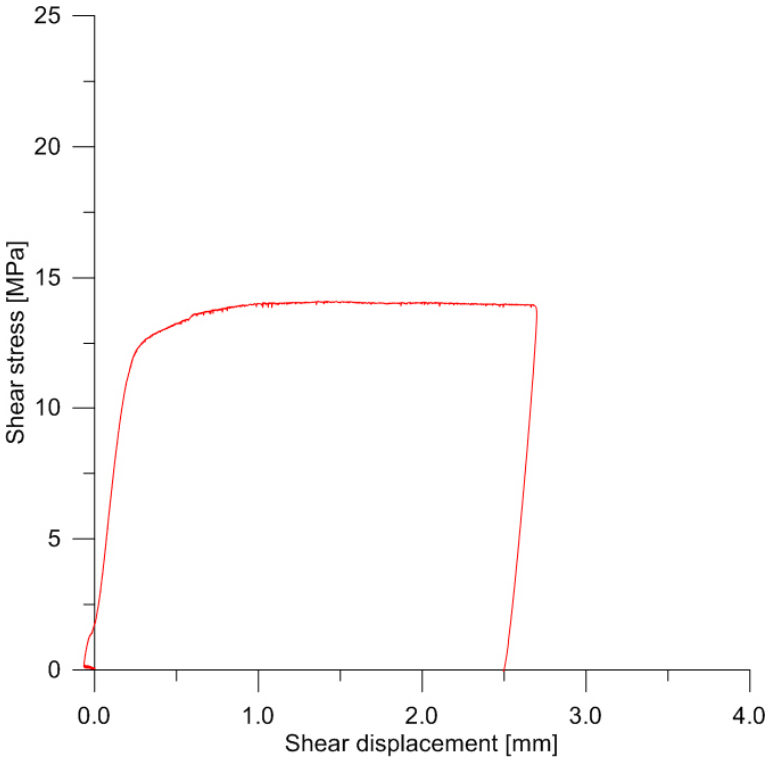

Figure C-23. *Shear stress vs. shear displacement for specimen DST-RCI-8 shear cycle s3.*

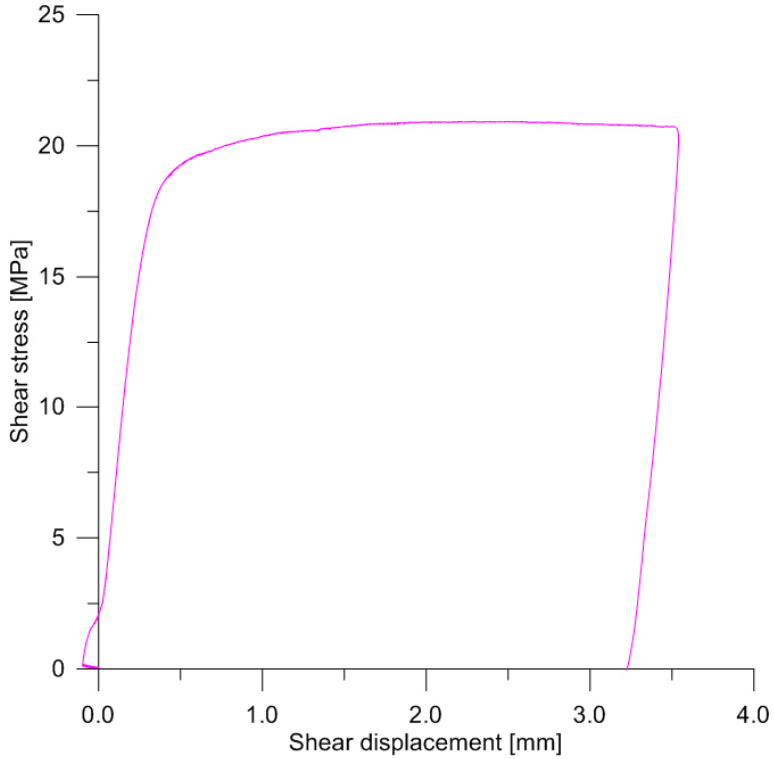

Figure C-24. *Shear stress vs. shear displacement for specimen DST-RCI-8 shear cycle s4.*

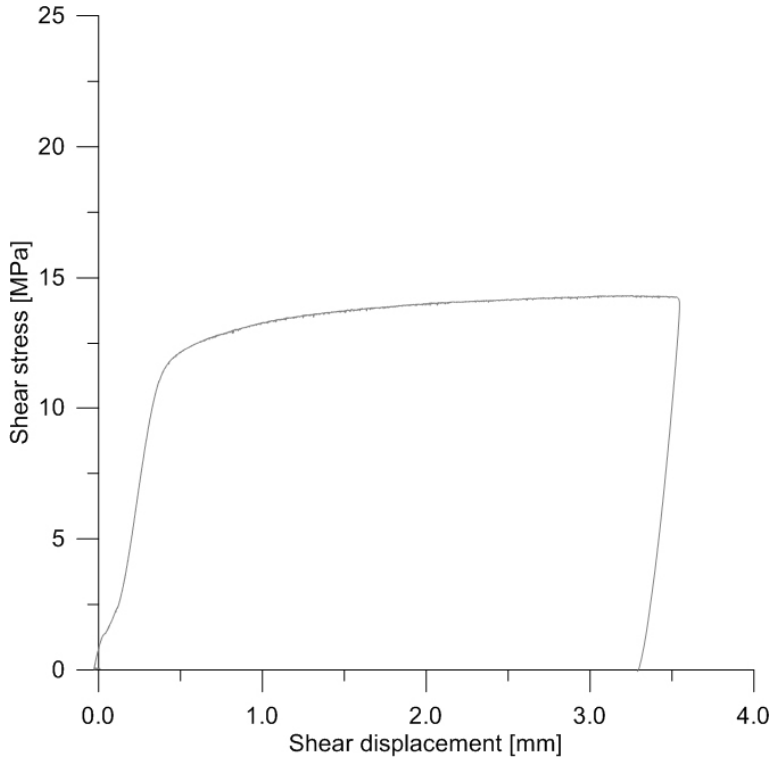

Figure C-25. *Shear stress vs. shear displacement for specimen DST-RCI-8 shear cycle s5.*

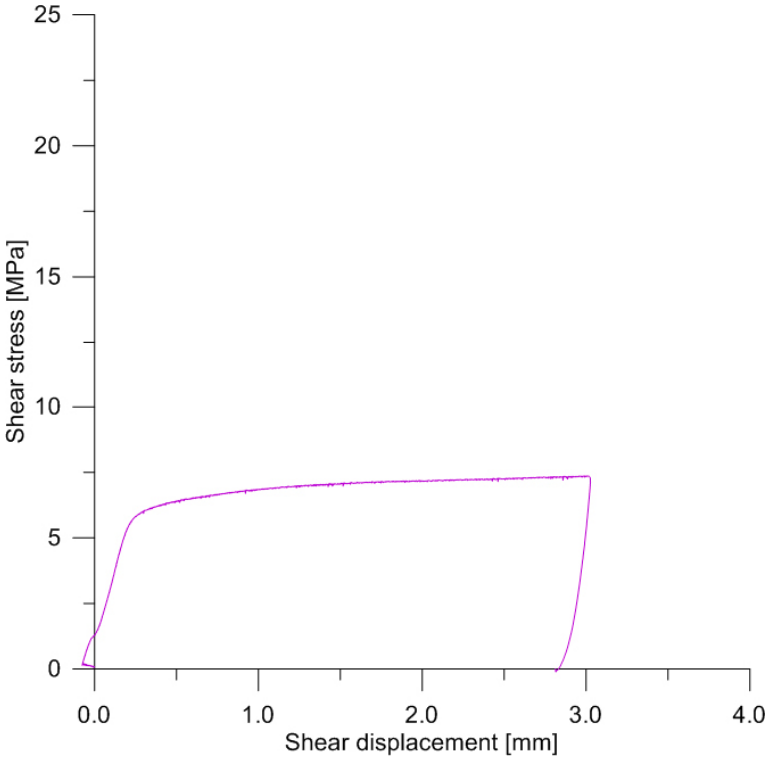

Figure C-26. *Shear stress vs. shear displacement for specimen DST-RCI-8 shear cycle s6.*

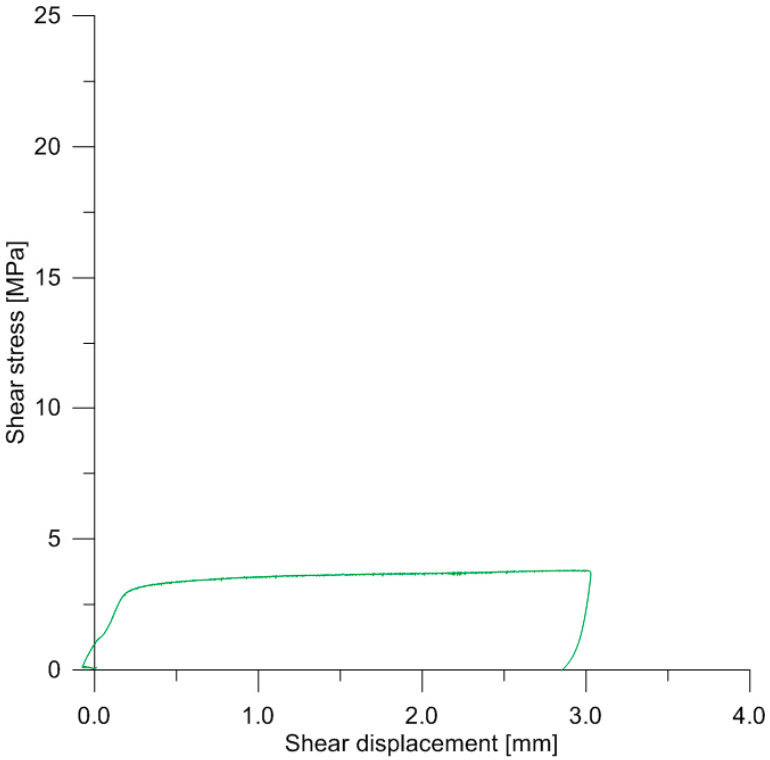

Figure C-27. *Shear stress vs. shear displacement for specimen DST-RCI-8 shear cycle s7.*

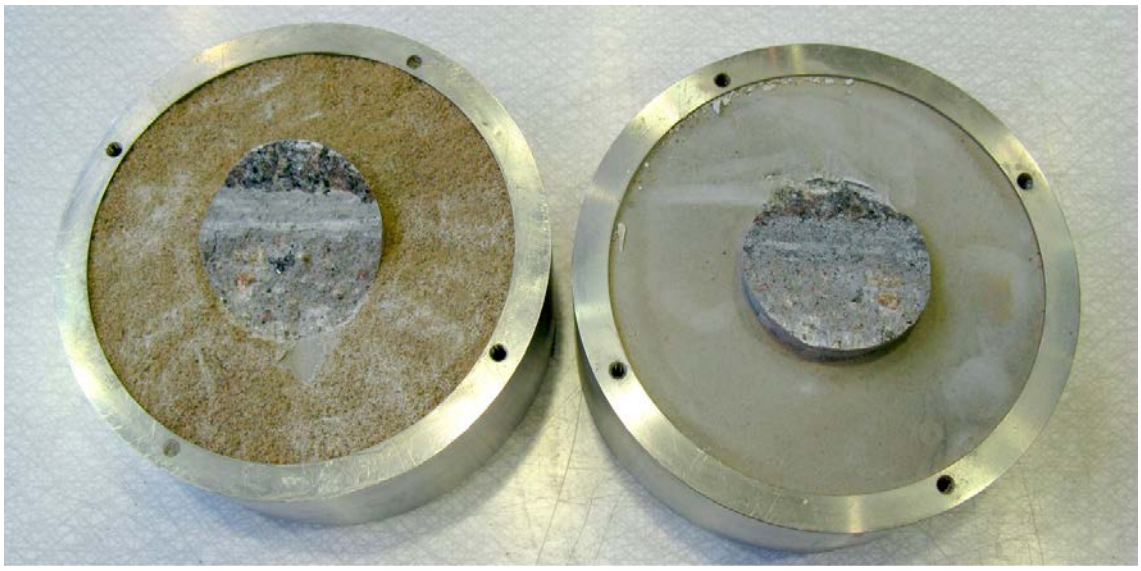

Figure C-28. *Photo of specimen DST-RCI-1 after testing.*

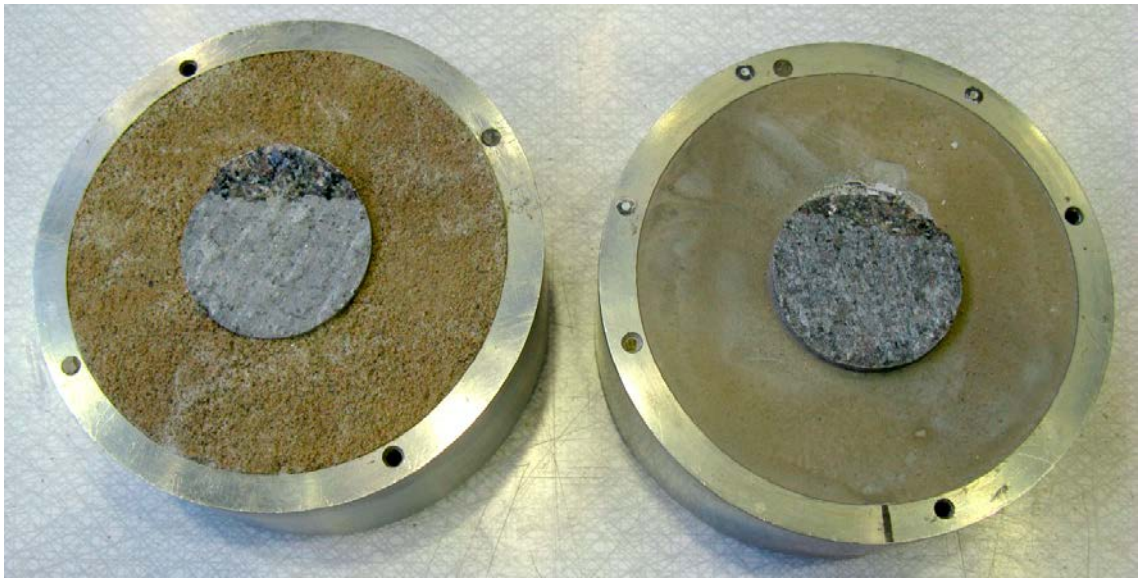

Figure C-29. *Photo of specimen DST-RCI-2 after testing.*

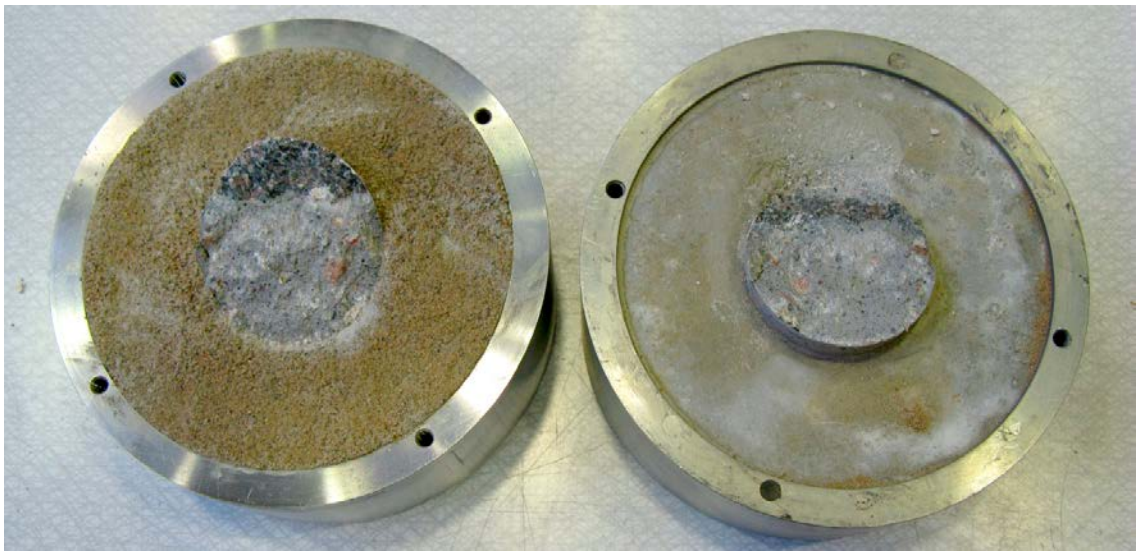

Figure C-30. *Photo of specimen DST-RCI-3 after testing.*

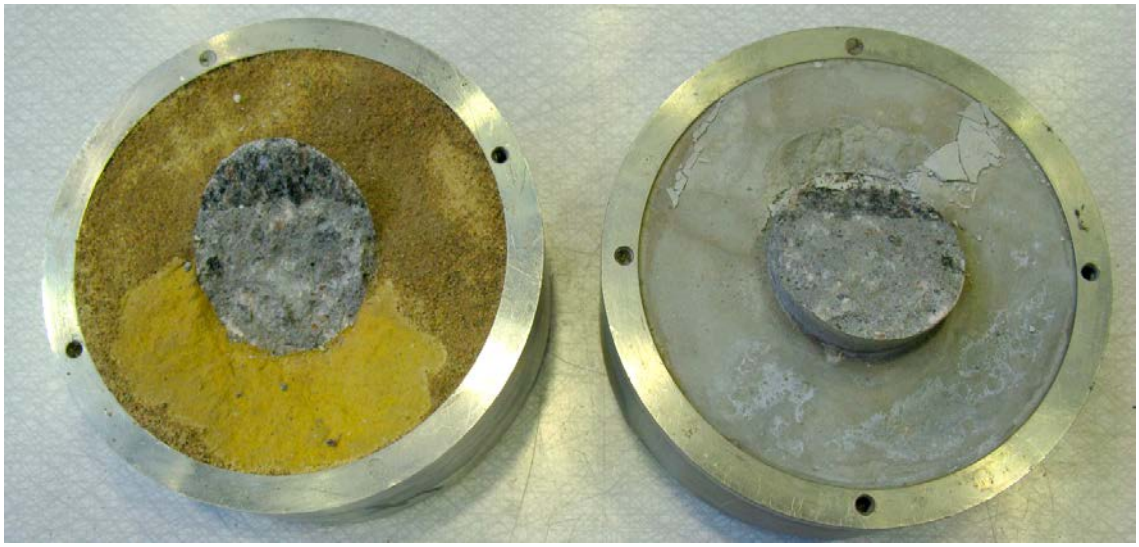

Figure C-31. *Photo of specimen DST-RCI-4 after testing.*

Figure C-32. *Photo of specimen DST-RCI-7 after testing.*

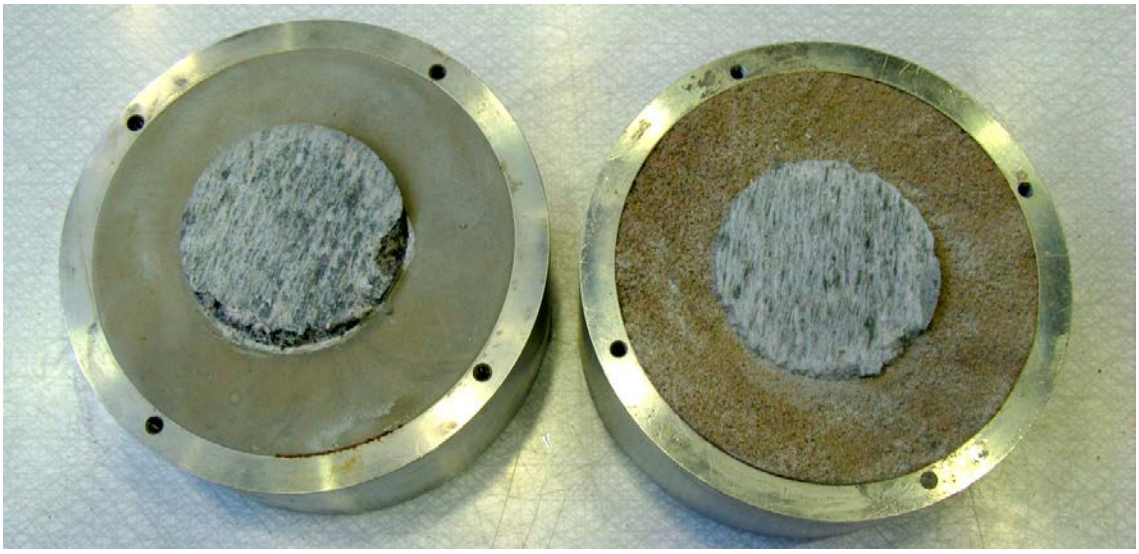

Figure C-33. *Photo of specimen DST-RCI-8 after testing.*